Prioritization in working memory reduces interference via a beta band-linked transformation of the not-selected item

Jacqueline M. Fulvio[1*], Bradley R. Postle[1,2]

[1]Department of Psychology, University of Wisconsin—Madison, Madison, Wisconsin, United States of America, 53705

[2]Department of Psychiatry, University of Wisconsin—Madison, Madison, Wisconsin, United States of America, 53719

*Corresponding author

Email: jacqueline.fulvio@wisc.edu (JMF)

Abbreviated title: Beta band-linked priority coding in working memory (50/50 chars)

Number of pages: 69

Number of figures: 7

Number of words in Abstract: 190

Number of words in Introduction: 918

Number of words in Discussion: 814

The authors declare no competing conflicts of interest.

Acknowledgements: This work was supported by NIH grant 1R01MH131678-01A1 to B.R.P

Abstract

We studied the effects of prioritization in a two-step retrocuing task in which male and female humans hold two items in working memory, and the item not cued by the first cue cannot be dropped because it may be prioritized by the second cue. In Experiment 1, using a dense sampling procedure, recall performance oscillated at 15 Hz in the prioritization task, in comparison to 20 Hz in a matched neutral-cue task. Furthermore, the prioritized item was shielded from bias exerted by the uncued item, as well as by items from the previous trial. In Experiment 2, we recorded the EEG while participants performed variants of the two tasks. The prioritization cue uniquely triggered a phase reset at 15 Hz and an increase in oscillatory peaks at this frequency. Burst analysis ruled out bursting as a possible underlying factor. Time-resolved representational similarity analysis (RSA) revealed that the prioritization cue triggered representational transformations that were larger for the uncued item. The shielding effects of prioritization may arise from the transformation of the not-prioritized item into an "unprioritized" state that is implemented and maintained by a mechanism that cycles at 15 Hz.

Significance statement **(117 / 120 words)**

When multiple items are held in working memory, the brain must prioritize the information currently needed to guide action while also managing the other information that remains potentially relevant for future actions. Through behavior and electroencephalography, we show that prioritizing one item in working memory shields it from interference from the not-prioritized item and that this shielding is implemented by

transforming the representational state of the unprioritized item. Behavioral signatures of this transformation and the underlying neural dynamics both cycle at a frequency in the low-beta band (~15 Hz). These findings suggest that the brain uses an oscillatory mechanism—distinct from previously described beta-bursting inhibitory control—to organize and protect the contents of working memory from inter-item competition.

Introduction

When multiple items are held in working memory, validly retrocuing the item that will subsequently be tested has consequences for behavior and for how this information is represented in the brain. Behaviorally, retrocuing results in higher accuracy and faster reaction times (as reviewed, e.g., by Hautekiet et al., 2025), effects interpreted as evidence that the cued item has become “more accessible” (Hautekiet et al., 2025). Neurally, retrocuing an item improves its decodability (interpreted as evidence for a “strengthening” of its neural representation, e.g., Sprague et al., 2016; Yu, Teng, & Postle, 2020), and transforms its representational geometry (Panichello & Buschman, 2021). One question that motivates the current study relates to the potential “shielding” effects of prioritization. Intuitively, one might assume that in addition to becoming “stronger,” the cued item might also become more resistant to the potentially interfering effects of other information being processed by the cognitive system, such as perceptual distractors. Empirically, however, evidence for such a “shielding” effect is mixed (as reviewed, e.g., by Hautekiet et al., 2025).

Importantly for the present report, the majority of studies that have used a retrocuing procedure have done so with tasks that only require a single response, thereby rendering the uncued item an “irrelevant memory item” (IMI) that can be “dropped” from working memory as soon as the cue has been processed. For example, in a recurrent neural network (RNN) simulation of the retrocuing task from Panichello & Buschman, (2021), after cuing, the IMI simply fades from working memory (Piwek et al., 2023). The focus in this report, in contrast, will be on a task in which the not-cued item

cannot be dropped from working memory because it might still be needed later in the trial.

An example of a situation in which the not-prioritized item cannot be dropped from working memory is the 2-back task, a continuous performance task in which each newly presented item in a series must be judged as a match or nonmatch of the item that had appeared two previously. While item *n* is on the screen, it serves as a recognition probe for item *n* – 2; next it becomes an “unprioritized memory item” (UMI) while *n* + 1 is being compared to *n* – 1; next it becomes the “prioritized memory item” (PMI) against which *n* + 2 is compared, and finally it becomes an IMI. In electroencephalography (EEG) data, the transition from probe to UMI is accompanied by the reversal of an item’s reconstruction by a multivariate inverted encoding model (IEM), a phenomenon equivalent to significantly below-chance decoding (Wan et al., 2022). In RNN simulation, the UMI and PMI are represented in ring manifolds that are reversed relative to one another, an item’s geometry underdoing a scalar flip during the transition from UMI to PMI (Wan et al., 2022), then, upon the transition to IMI status, collapsing to a scalar value undifferentiable from 0 (i.e., “fading until no trace remains”; Wan et al., 2022). These considerations highlight two factors that provide important motivation for the present studies. First, they highlight that the nature of possible shielding effects bestowed by prioritization may be very different for tasks in which the UMI cannot be dropped from working memory (in comparison to single-cue tasks like those summarized above). Second, in addition to perceptual distractors, a potentially important source of interference in cannot-drop-the-UMI tasks is, indeed, the UMI. To our knowledge, no previous studies of interference between items concurrently held in

working memory (what we will refer to as “within-trial” interference) have examined the effects of prioritization.

The research presented here uses variants of a double serial retrocuing (DSR) task, in which the presentation of two sample items is followed by an initial retrocue, then an initial test of recall, then a second retrocue, then a second test of recall. Although initial work with the DSR task had suggested that an item might transition into an “activity-silent” state upon being designated a UMI by the initial cue (e.g. Lewis-Peacock et al., 2012; Rose et al., 2016), more recent findings (Yu, Teng, & Postle, 2020) indicate that the UMI can undergo a representational transformation similar to what has been reported with the 2-back task (Wan et al., 2022). Additionally, and of particular relevance for this report, is the fact that previous work with the DSR task has also implicated a possible role for oscillations in the beta band: beta-band dynamics relate to the effects of transcranial magnetic stimulation (TMS) on behavior (Fulvio et al., 2024), and they make selective contributions to decoding the identity of the UMI (Rose et al., 2016; Fulvio & Postle, 2025). Previous working memory research has highlighted at least two distinct mechanisms operating in the beta band. One is phase encoding, whereby each of two items in working memory is held at a different phase angle in ongoing theta-band (~6 Hz) and beta-band (~25 Hz) oscillations (Abdalaziz et al., 2023). A second is that, in a manner analogous to the stopping of skeletomotor actions (Diesburg et al., 2021; Hervault & Wessel, 2025), bursts in the beta frequency range may provide a mechanism for imposing top-down control on the processing of information in working memory (Lundqvist et al., 2024). The research presented here was also designed to assess whether the beta-band dynamics associated with

prioritization in the DSR task (Rose et al., 2016; Fulvio et al., 2024; Fulvio & Postle, 2025) may correspond to phase encoding (Abdalaziz et al., 2023), to bursty top-down control (Lundqvist et al., 2024), or to a third previously undescribed phenomenon.

Experiment 1

Materials & methods

Participants

Eighteen neurologically healthy members of the University of Wisconsin–Madison community participated in the behavioral experiment. Incomplete data sets from two participants were excluded yielding a final sample of 16 data sets used in the analyses (from 10 females, 2 unknown, 18-32 years, *M* = 22.8 years). The sample size was chosen to match the sample size of Bae & Luck (2017), which reported the inter-item bias effects we aimed to replicate and understand here. All participants had normal or corrected-to-normal vision, and all reported having normal color vision. The research was approved by the University of Wisconsin—Madison Health Sciences Institutional Review Board. All participants gave written informed consent at the start of the session and received monetary compensation in exchange for participation.

Experimental procedure

Double serial-retrocue task. The double serial-retrocue (DSR; **Fig. 1A**) task began with the 200 ms presentation of an oriented grating at the center of the display ("*Sample 1*"), followed by a 500 ms inter-stimulus fixation interval ("*ISI*"), followed by the 200 ms presentation of a second oriented grating at the center of the display ("*Sample 2*"), followed by 500 ms of fixation ("*Delay 1.1*"), followed by a 500 ms presentation of *Cue 1* (the digit '1' or '2') whose value indicated with 100% validity which of the two

samples would be tested. This cue conferred on the cued item the status of the prioritized memory item (PMI) and, by default, the uncued item took on the status of unprioritized memory item (UMI). *Cue 1* was followed by a fixation period ("*Delay 1.2*") of variable length, densely- and uniformly-sampled across a range from 500-1200 ms in steps of 16.67 ms, implemented in the code as number of screen refreshes. *Delay 1.2* was followed by *Recall 1* in which a circle with a line corresponding to its diameter (and described to participants as a "dial") was presented. Using the mouse, participants rotated the line to match the orientation of the cued item and clicked the mouse button to lock in their response within a 3-sec window beginning with probe onset. Feedback was displayed for the 1 second interval following the 3 second recall interval, the fixation cross turning green for responses less than 20 deg from the sample orientation, yellow for responses between 20 and 28 deg from the sample orientation, and red for responses greater than 28 deg from the sample orientation. If no response was recorded, the words "No response was recorded" appeared during the feedback interval. The trial then continued with a 500 ms presentation of *Cue 2* (the digit '1' or '2') whose value indicated with 100% validity which of the two samples would be tested during *Recall 2*. The item designated by *Cue 2* took on the status PMI, and the uncued item the status of irrelevant memory item (IMI; because it could no longer be cued on that trial). *Recall 2* and feedback periods were identical to *Recall 1* and its feedback period. After feedback to *Recall 2*, text appeared at the center of the display telling the participant to press the spacebar key when ready to continue with the next trial. This triggered the inter-trial interval, which varied between 2-3 s ("*ITI*"). Upon completion of the block, text appeared on the display informing the participant of their average recall

error in degrees on that block. Over the course of each block, *Cue 2* indicated the same item as had *Cue 1* on 50% of trials ("*stay*" trials; the remaining 50% were "*switch*" trials).

Neutral-cue task. The neutral-cue (NEU; **Fig. 1B**) task was identical to the DSR task with two exceptions: (i) trials featured only one *Cue* and one *Recall* and *Feedback* period; and (ii) the *Cue* was uninformative, appearing as '0' on each trial. Throughout the text, we will refer to the items in the NEU task not as PMI and IMI, but rather as "tested" and "untested."

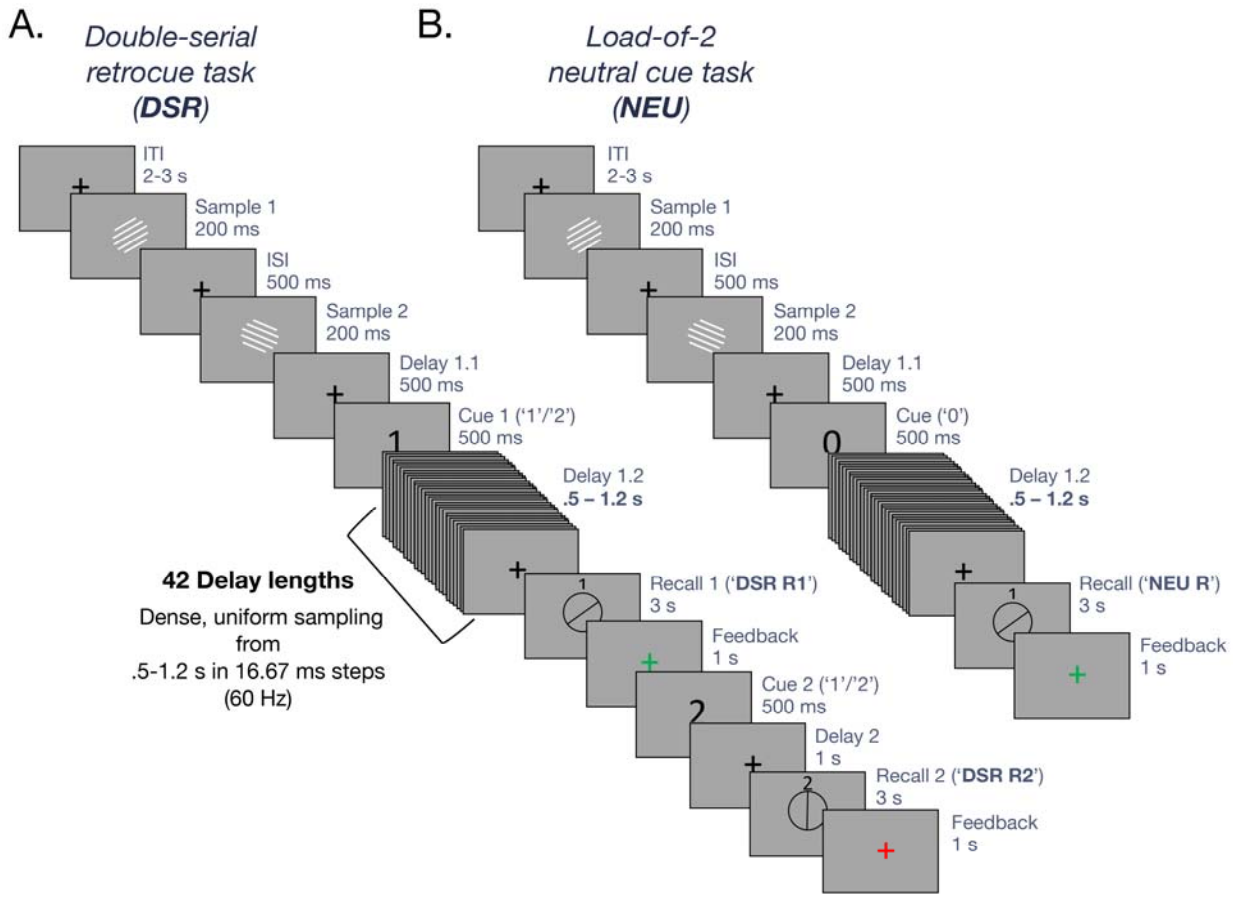

Fig 1. Experiment 1 behavioral task schematics. A. Schematic of the double-serial retrocue (DSR) task. Participants memorized the identity of two centrally presented oriented grating samples shown at successive time points with an intervening delay ('*ISI*'). Partway through the delay (i.e., at the end of *Delay 1.1*) an ordinal retrocue indicated which of the two items would be tested, after the ensuing *Delay 1.2* of variable length, sampled uniformly from .5-1.2 s in 16.67 ms increments. At test (*Recall 1*), participants rotated the recall dial with the mouse to the orientation of the tested sample item in memory. After feedback, a second ordinal retrocue (*Cue 2*) indicating which of the two samples would be tested during *Recall* 2 followed by a final delay. **B.** Schematic of the load-of-2 neutral cue (NEU) task, which followed the same task structure as the DSR task through the first feedback interval, after which the trial ended. Importantly, an uninformative '0' was presented during the cue interval, preventing participants from anticipating which item would be tested at recall.

Experimental stimuli and design

Participants were seated in a dimly lit room at a viewing distance of 50 cm from the monitor. Sample stimuli were centrally presented black and white gratings appearing on a mid-gray background with radii of 6°, spatial frequencies equal to 1 cycle/°, 50% contrast, and random phase. The orientation of one of the sample items was selected from a set of six base orientations (10, 40, 70, 100, 130, 160°), with a random jitter of −3° to 3°. The orientation of the other sample item was selected to be offset from the jittered base orientation from a set of inter-item angular differences (0, +/-22.5, +/-45, +/-67.5°). The presentation order of the base orientation and offset orientation was randomized and counter-balanced across trials. The centrally presented cues were black digits, and the recall stimuli were black response dials (unfilled black circles with a black line corresponding to the diameter of the circle) with the same radius and random starting orientation. A fixation cross was presented during blank task intervals. The cross was gray during the fixation and *ISI* intervals, white during the memory delay periods, and green, yellow, or red during the feedback interval, depending on the response error.

The experiment was completed in a single session, and all participants completed four blocks of the DSR task followed by four blocks of the NEU task. (We reasoned that participants were less likely to ignore DSR cues if they had not previously performed a variant of the task with uninformative cues.) Prior to each set of four blocks, participants completed 8-12 practice trials of the task in the presence of the experimenter. During practice trials, the feedback display differed. After the participant locked in their recall response, the recall stimulus remained on the display and changed

color according to the green/yellow/red feedback convention, and the original sample grating reappeared under the recall stimulus to provide visual error feedback to the participant during these trials.

Each block was comprised of 84 trials for a total of 336 trials per task, and participants were encouraged to take breaks between blocks (and between trials if necessary) before continuing. Any trial for which a response was not recorded within the 3-second window was repeated at the end of the block. Because we were primarily interested in behavioral oscillations (and hence the manipulation of the duration of *Delay 1.2*), we established the experimental design to ensure an equal number of trials collected for each of 42 durations of *Delay 1.2*. This resulted in 8 trials collected at each duration, of which there were 2 trials per inter-item angular difference (magnitude) collected per task, per participant. Across those, the base orientations were randomly sampled such that each base orientation was selected for an equal number of trials across all possible base orientation values, but they were not equated across *Delay 1.2* durations.

Behavioral analyses

Mean absolute error of recall. For both DSR and NEU tasks, we quantified overall accuracy of recall by computing the average magnitude of the angular difference between the participant's recall response value and the orientation of the tested sample item, as a function of inter-item angular difference and, for the second response of the DSR task, as a function of 'stay'/'switch' identity of *Cue 2*. We also tested for differences in absolute recall error as a function of the target's presentation order (i.e., as *Sample 1* or *Sample 2*). Paired-sample *t*-tests were used to test for significant differences in mean

absolute error of recall across task responses with Bonferroni correction for the number of tests. A linear mixed effects model was used to test for a significant effect of task (2 levels: DSR/NEU, coded as a categorical variable) and inter-item angular difference magnitude (4 levels: 0, 22.5, 45, 67.5 deg). In the model that is reported here, the task x inter-item angular difference interaction term was omitted because this interaction was found to be non-significant and inclusion of the term did not significantly improve the model fit. Subject was included as a random effect, and a separate intercept was fitted for each.

Inter-item bias. Following Bae & Luck (2017), we quantified the bias exerted by the untested item on the recall of the tested item as the mean signed recall error, with negative signed errors indicating attraction and positive signed errors indicating repulsion. For each trial, we computed the recall error, and if the response value was in the direction of the untested item, the recall error was given a negative sign, and if the response value was in the direction away from the untested item, the recall error was given a positive sign. As with mean absolute error, we quantified the inter-item bias for both responses during the DSR task and the single response during the NEU task, as well as separately for the second response of the ‘stay’ and ‘switch’ trials of the DSR task, and as a function of inter-sample item angular difference. Paired-sample *t*-tests were used to test for significant differences in inter-item bias across task responses with Bonferroni correction for the number of tests. A linear mixed effects model was used to test for a significant effect of task (2 levels: DSR/NEU, coded as a categorical variable) and inter-item angular difference magnitude (4 levels: 0, 22.5, 45, 67.5 deg) and their

interaction with subject included as a random effect and a separate intercept fitted to each.

Serial dependence. In addition to within-trial inter-item effects on recall, we also tested for between-trial inter-item effects on recall. For each participant's data, the response error on each trial was computed as the angular distance between the presented and reported sample orientation. Following previous serial dependence work (Bliss et al., 2017; Fritsche et al., 2017; Samaha et al., 2019; Fulvio et al., 2023), high-error trials (≥25 deg; *M* = 5.4%) were omitted from analysis. To remove any global directional biases of individual participants, we subtracted their mean signed error across trials from each trial. Serial dependence was quantified by sorting each participant's demeaned errors according to the angular difference between the sample direction on the current and previous trials. Here, we quantified serial bias exerted by the previous trial's most recent PMI/tested item (i.e., with respect to the PMI designated by *Cue 2* in DSR trials), as well as the bias exerted by the previous trial's IMI/untested item. In these analyses, the first trial of each block was omitted. For instances in which trials were removed due to large errors, the most immediately preceding non-large error trial served as the previous trial. The sorted errors for each participant were then smoothed by a 20°-wide median filter in 2° increments. (Similar results were obtained with different-sized filters.)

We averaged the smoothed data within each condition and fit the averages of each with a von Mises–based function of the following form:

$$y = a\ \sin(2x)\ e^{\mathrm{k}\cos(2x)} \qquad (1)$$

where x is the relative orientation of the tested/untested item of the previous trial (in radians), a is the amplitude of the curve, and k is the concentration parameter determining the width of the tuning. The sine and cosine terms capture the circular periodicity of orientation differences over 180°, allowing the function to model both attractive and repulsive serial biases symmetrically around zero (analogous to a derivative-of-von-Mises (dVM) formulation used in previous studies; e.g., Fritsche et al., 2017). Fitting was achieved by minimizing the sum of squared errors using the *lsqcurvefit* MATLAB routine, with amplitude a and concentration k parameters free to vary between –10° and 10° and between 0 and 10, respectively.

Statistical significance of the group-level dVM fits was assessed through a bias-corrected and accelerated (BCa) bootstrapping procedure. On each of 100,000 iterations, we sampled participants' data with replacement and fit a dVM to the average of the bootstrapped sampled data. The value of the amplitude parameter was retained after each iteration, resulting in a distribution of the amplitude parameter of our sample. We also computed the jackknife distribution of amplitude parameters by computing all of the leave-one-sample-out dVM fits. The confidence interval and *p*-value of the amplitudes of each group fit when compared to zero (i.e., no serial dependence) were computed using the BCa_bootstrap MATLAB function (van Snellenberg, 2018), which utilized both the bootstrapped and jackknife amplitude distributions.

Between-condition comparisons of dVM fit amplitudes were carried out using permutation testing. On each of 100,000 iterations, we shuffled the group labels (e.g., 'DSR' / 'NEU'; 'PMI' / 'IMI') and then assigned each dataset with one of the shuffled labels. We then grouped the data by the shuffled labels and fit a dVM to the average of

each shuffled group. The value of the amplitude parameter was retained after each iteration, resulting in a permutation distribution of the amplitude parameter. The *p*-value of the original difference in amplitudes between the two groups was derived from the permutation distribution as the proportion of the permutations greater than the original difference.

Linear mixed effects modeling of inter-item effects. After the data were collected, the separate analyses of inter-item influences on recall, as described in the previous section, revealed interference from both current-trial and previous-trial memory items (see **Supplementary Figure S2** for more detail). Because of this, we fit the data from each task to a linear mixed effects model to simultaneously model the inter-item biases of current and previous trial sample items on current trial recall. The dependent variable was the signed recall error on the current trial, modeled as a function of (i.) the orientations of the previous trial's tested item, (ii.) the previous trial's untested item, and (iii.) the current trial's untested item. Specifically, the predictors were derived from the difference between each item's orientation (in radians) relative to the current trial's target orientation, computed using the *circ_dist.m* function to ensure proper angular wrapping, and transformed using the sine of twice the angle, $\sin(2\theta)$, to capture orientation-dependent modulations in a directionally signed space. An additional categorical predictor ('NonTargetPresentation') coded whether the current trial's untested item was presented before (1) or after (0) the target item, to assess whether temporal order of presentation modulated inter-item bias. The model took the following form:

$$\text{Recall Error} \sim \sin(2*\theta_{\text{prev_tested}}) + \sin(2*\theta_{\text{prev_untested}})$$

$$+ \sin(2*\theta_{\text{curr_untested}}) * \text{NonTargetPresentation} + (1 \mid \text{Subject}) \quad (2)$$

Subject was included as a random effect, with random intercepts to account for inter-individual variability. This model was selected based on nested model comparisons in fitting the NEU data and then used to separately model both the NEU and DSR task *Recall 1* data.

A third model was fit to directly compare the within-trial biases of the two tasks with the form:

$$\text{Recall Error} \sim \text{Task}* (\sin(2*\theta_{\text{prev_tested}}) + \sin(2*\theta_{\text{prev_untested}})$$

$$+ \sin(2*\theta_{\text{curr_untested}}) * \text{NonTargetPresentation}) + (1 \mid \text{Subject}) \quad (3)$$

where Task was included as a categorical variable, with the DSR task dummy-coded to be the reference task. This model included the three-way interaction between Task, the current trial's untested item, and the presentation order of the current trial's untested item to test whether the effect of prioritization on inter-item bias depended on temporal order of presentation.

After model fitting, we extracted the fixed effects estimates and their associated 95% confidence intervals. Standard errors were computed from the confidence interval widths, and *t*-statistics were obtained as the ratio of each fixed-effect estimate to its standard error. Corresponding two-tailed *p*-values were then derived from the *t* distribution using the model's residual degrees of freedom. Importantly, positive coefficients for the sine-transformed predictors would indicate attractive biases toward them, whereas negative coefficients would indicate repulsive biases away from them.

To directly test whether the magnitude of inter-item angular difference modulated bias, we conducted a supplementary analysis using a signed bias measure as the

dependent variable. This measure was computed by multiplying the signed recall error by the sign of the angular difference between the current trial's untested and target items, such that positive values indicate attraction toward the untested item and negative values indicate repulsion away from it, maintaining consistency with the primary LME analyses above. The 25% of trials with 0° angular difference were excluded from this analysis because signed bias is undefined when the two items are identical.

The signed bias was modeled as a function of (i.) the angular difference between the current trial's items (22.5°, 45°, or 67.5°; treated as a categorical variable), (ii.) the presentation order of the current trial's untested item, and (iii.) their interaction, while controlling for previous trial influences using the sine-transformed orientation differences of the previous trial's tested and untested items. The model took the following form:

$$\text{Signed Bias} \sim \text{AngDiff} * \text{NonTargetPresentation} + \sin(2*\theta_{\text{prev_tested}}) + \sin(2*\theta_{\text{prev_untested}}) + (1 \mid \text{Subject}) \quad (4)$$

Subject was included as a random effect with random intercepts to account for inter-individual variability. This model was fit separately to the NEU and DSR task data.

A third model was fit to directly compare the effects of angular difference across tasks with the form:

$$\text{Signed Bias} \sim \text{Task} * (\text{AngDiff} * \text{NonTargetPresentation}) + \sin(2*\theta_{\text{prev_tested}}) + \sin(2*\theta_{\text{prev_untested}}) + (1 \mid \text{Subject}) \quad (5)$$

where Task was included as a categorical variable, with the DSR task dummy-coded as the reference level. This model tested whether the effect of angular difference on inter-item bias, and its interaction with presentation order, differed between tasks.

Behavioral oscillations. Behavioral oscillations in recall were assessed by analyzing mean absolute error (MAE) as a function of *Delay 1.2* duration (0.5–1.2 s, 42 discrete intervals). For each participant and duration, MAE values were averaged across trials and smoothed with a two-point moving average. The resulting delay-dependent MAE series was linearly detrended to remove slow drifts. To detect rhythmic fluctuations in performance, a Fast Fourier Transform (FFT) was applied to each participant's detrended MAE time series. Prior to transformation, data were multiplied by a Hann window to reduce spectral leakage and zero-padding to the nearest power of two was applied for computational efficiency and to interpolate the frequency spectrum. The FFT yielded complex coefficients representing amplitude and phase values across 33 frequency bins spanning 0–30 Hz. Group-level spectra were obtained by averaging participants' complex Fourier coefficients (real and imaginary components), preserving the relative phase information across participants. This approach ensures that consistent phase alignment across participants contributes to the group-level amplitude, rather than being lost through power-only averaging. To assess statistical significance, *Delay 1.2* trial labels were randomly shuffled for each participant, after which delay-dependent MAE was recomputed and the FFT was repeated. This procedure was performed 10,000 times to generate participant-wise null spectra and corresponding group-level amplitude distributions. Observed spectral peaks exceeding the 95th percentile of the null distribution—corrected for multiple comparisons (Bonferroni correction was applied across identified peaks)—were considered significant and would indicate rhythmic modulation of behavioral performance at the frequencies of the significant peaks.

For frequencies showing significant oscillatory peaks, between-participant phase alignment was quantified using the Phase-Locking Value (PLV). To compute this, each participant's phase angle at their peak frequency was extracted from the complex FFT output, and PLV was computed as the absolute value of the mean complex phase vector:

$$PLV = \frac{1}{N}\sum_{n=1}^{N} e^{i\theta_n} \qquad (6)$$

where N is the number of participants, θ_n is the phase angle for participant n, and $i = \sqrt{-1}$. *PLV* values range from 0 (uniform phase distribution) to 1 (perfect phase alignment). Statistical significance of phase alignment was assessed using both a parametric Rayleigh test for non-uniformity and a non-parametric permutation test. For the latter, *PLV* values were computed for each of the 10,000 permutation-based null datasets, and the observed *PLV* was compared to the resulting null distribution (α=0.05).

All analyses were conducted separately for the DSR and NEU tasks, allowing for direct comparison of peak oscillation frequencies between tasks. Identical procedures were repeated to assess oscillations in within-trial inter-item bias on recall.

Results

Recall accuracy

Mean absolute error (MAE) of recall did not differ between DSR *Recall 1* and NEU recall ($t(15) = 0.6046$, $p = .555$), whereas the MAE of DSR *Recall 2* was significantly larger than for DSR *Recall 1* and NEU recall (both p-values < .01; **Fig. 2A**). No difference was observed between the MAE of DSR *Recall 2* for 'stay' versus 'switch' trials ($t(15)$ =

0.0526, $p = .959$; **Supplementary Figure 1A**). Larger inter-item angular differences were associated with larger errors, with a linear mixed effects model confirming a significant main effect of current trial inter-item angular difference on performance ($F(1,189) = 140.81$, $p < .001$; **Fig. 2B**). When the model included both recall responses of the DSR task, a significant main effect of task was also observed ($F(1,189) = 9.9764$, $p = .002$), driven by the worse performance for *Recall 2* of the DSR task (see also **Supplementary Figure 1B**).

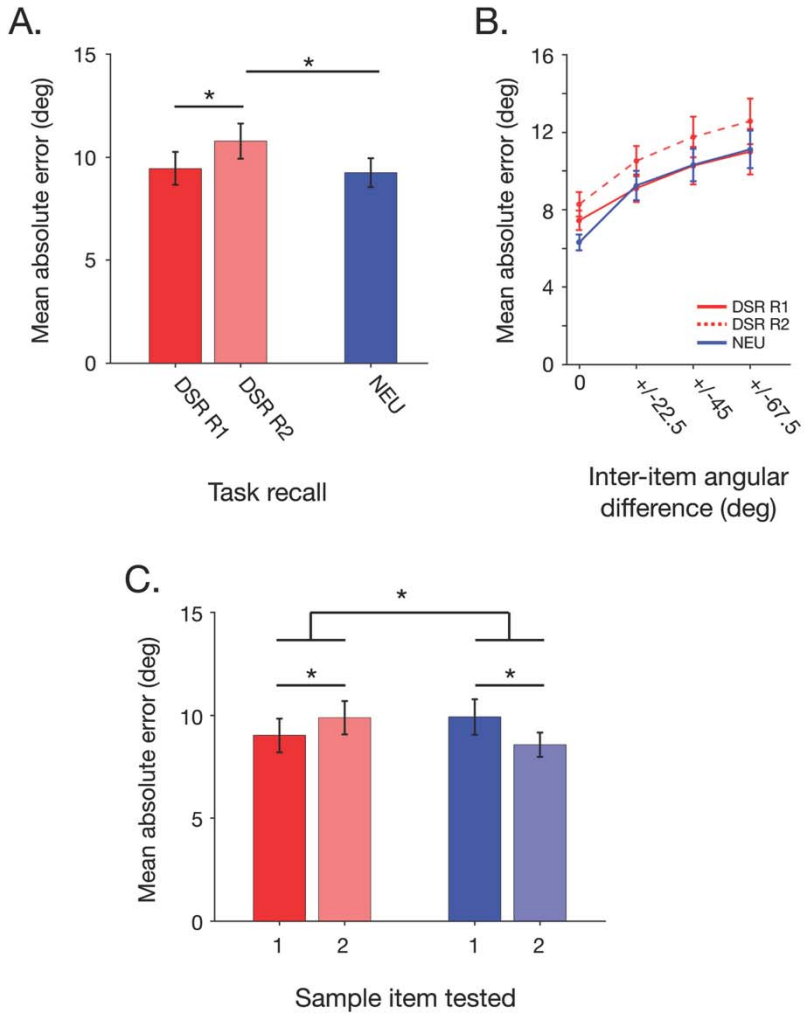

Fig 2. Experiment 1 recall accuracy. A. Mean absolute recall error for the two responses of the DSR task and the single response of the NEU task. **B.** Same as **A.** separated by the current trial's inter-item angular difference. **C.** Mean absolute error for DSR *Recall 1* and NEU recall as a function of which item was tested (*Sample 1* vs. *Sample 2*). Error bars correspond to +/- 1 *SEM.* * symbols correspond to significant differences between conditions at the Bonferroni-corrected alpha level = .0167 for 3 paired-sample *t*-tests (**A.**) and the Bonferroni-corrected alpha level = .025 for two paired-sample *t*-tests and for interaction $p < .05$ (**C.**).

Finally, comparison of MAE as a function of the presentation order of the PMI/tested item revealed different patterns between NEU recall and DSR *Recall 1*: In NEU, MAE was significantly smaller when *Sample 2* was tested ($t(15) = 2.805$, $p = .0133$), whereas in DSR, MAE was significantly smaller when *Sample 1* was tested ($t(15) = -2.734$, $p = .0154$); **Fig. 2C**). This pattern resulted in a significant performance crossover between the two tasks ($t(15) = -3.849$, $p = .0016$).

Across- and within-trial bias

Linear mixed effects modeling revealed that response error was systematically influenced by both the previous trial's tested item and the current trial's untested item, with the latter effect dependent on the order of presentation (**Supplementary Table S1**). In both tasks, the previous trial's tested item exerted an attractive bias on recall (NEU: $\beta = 1.08°$, $p < .001$; DSR: $\beta = 0.84°$, $p = 0.002$), an effect that did not differ across task ($\beta = 0.25°$, $p = .517$; **Supplementary Table S2**). The previous trial's untested item had no significant effect on recall. Turning to within-trial effects, recall of *Sample 1* was attracted toward the value of *Sample 2* for NEU ($\beta = 3.55°$, $p < .001$) and for DSR ($\beta = 1.66°$) but recall of *Sample 2* showed no significant bias in NEU ($\beta = 0.08°$, $p = .818$) or DSR ($\beta = 0.50°$, $p = .177$). The three-way interaction between task, current-trial untested item, and order-of-presentation was significant ($\beta = –2.31°$, $p = .002$; **Supplementary Table S2**), confirming that the effect of prioritization was to reduce the influence of *Sample 2* on the recall of *Sample 1*.

Linear mixed effects modeling further revealed that inter-item angular difference significantly modulated bias ($F(2,3977) = 7.16$, $p < .001$; **Supplementary Table S3**) in the NEU task, and this effect interacted with order of presentation ($F(2,3977) = 6.35$, $p =$

.002). Recall of *Sample 1* was significantly attracted toward *Sample 2* at small and medium angular separations (22.5°: 3.68°, $p < .001$; 45°: 3.72°, $p < .001$), with attraction reduced to a marginally significant level at the large angular separation (67.5°: 1.09°, $p = .052$; a significant reduction from the bias at 22.5: $\beta = -2.59°$, $p = .001$). Recall of *Sample 2*, in contrast, showed no significant bias relative to *Sample 1* at any angular separation (22.5°: -0.42° $p = .461$; 45°: 0.01° $p = .987$; 67.5°: 0.63° $p = .251$). The main effect of presentation order was significant ($F(1,3977) = 26.72$, $p < .001$). In DSR, bias was small and the pattern of bias did not vary significantly across inter-item angular differences ($F(2,3975) = 0.70$, $p = .499$) nor was there an interaction of inter-item angular difference interaction with order of presentation ($F(2,3975) = 1.65$, $p = .192$). Recall of *Sample 1* was attracted to *Sample 2* at medium and large angular separations (45°: 1.76°, $p = .002$; 67.5°: 1.42°, $p = .013$) but not at the small separation (22.5°: 0.81°, $p = .155$). Recall of *Sample 2*, in contrast, showed no significant bias relative to *Sample 1* at small and medium angular separations (22.5°: -0.71°, $p = .208$; 45°: 0.22°, $p = .698$), but attraction at the large angular separation (67.5°: 1.67°, $p = .003$). Importantly, the previous trial's target, which exerted a significant attractive bias on recall in the primary analysis, did not significantly influence signed bias in either task. This indicates that the previous trial's influence operated separately in absolute orientation space, pulling responses toward the previous target's orientation, rather than by influencing interactions between the current trial's items.

The task comparison model confirmed that NEU showed significantly greater overall bias than DSR ($F(1,7954) = 12.98$, $p < .001$), and that the effect of angular

difference was significantly larger in NEU than DSR (interaction: $F(2,7954) = 4.21$, $p = .015$; **Supplementary Table S4**).

Behavioral oscillations

Permutation-based FFT analysis revealed significant rhythmic fluctuation of mean absolute error, at different frequencies, on both tasks (**Fig. 3A**). DSR showed significant behavioral oscillatory peaks clustered around 15 Hz (14.06, 15.00, and 15.94 Hz), with the dominant frequency at 15.00 Hz (amplitude = 0.34 degrees). The NEU task exhibited significant behavioral oscillations with the dominant frequency at 20.62 Hz (amplitude = 0.18 degrees; range = 19.69 and 20.62 Hz). Participant-level peak frequency analysis confirmed that the peak oscillatory frequencies differed significantly between conditions ($M = 5.15$ Hz; *95% CI*: [3.38, 6.93] Hz; $t(15) = -6.18$, $p < 0.001$). From here forward, to relate them to the classical frequency band of EEG oscillation, we will refer to these two frequencies as “low-beta” and “higher-beta,” respectively.

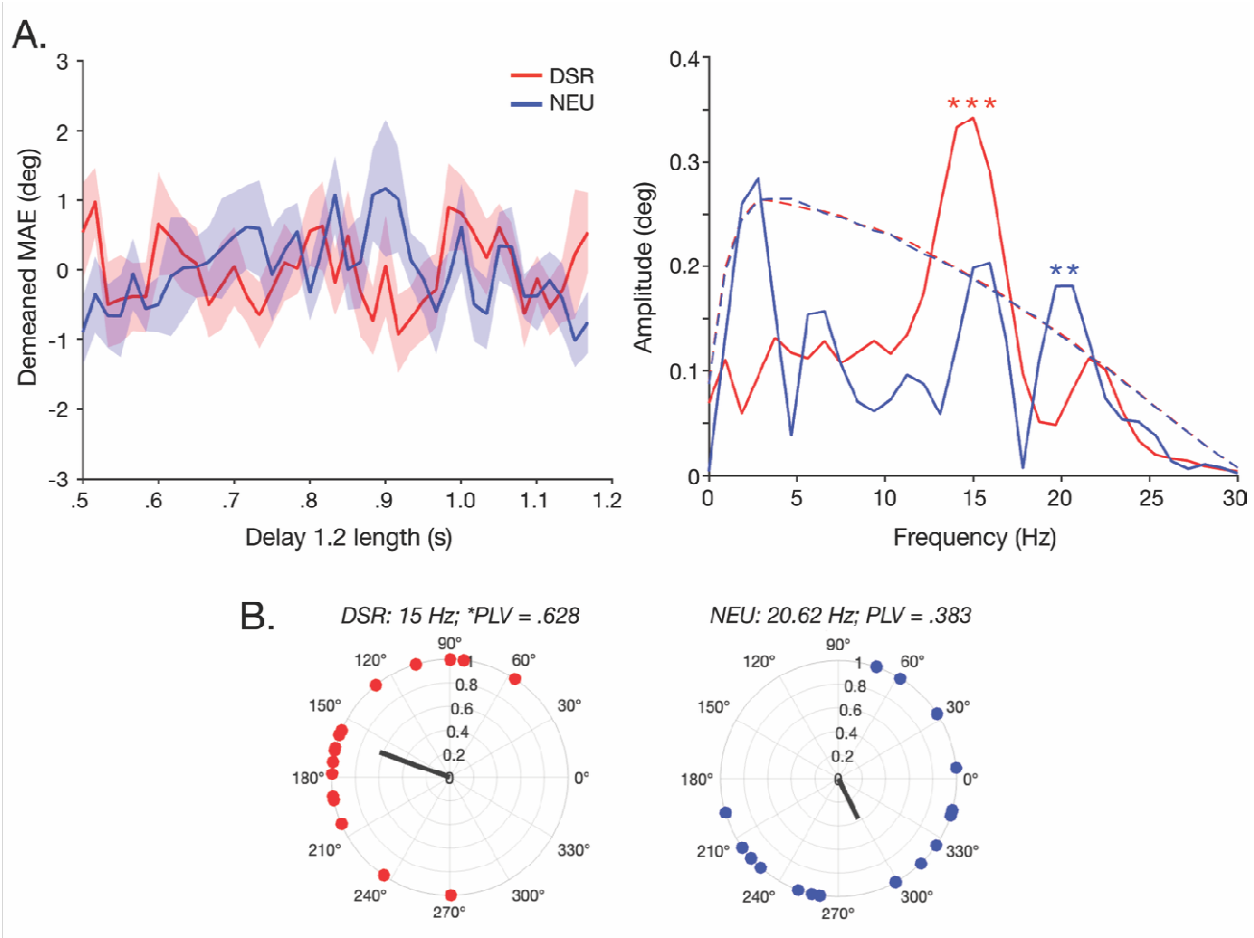

Fig 3. Experiment 1 behavioral oscillations of mean absolute error. A. Demeaned mean absolute recall error for DSR R1 (red) and the single response of the NEU task (blue) as a function of Delay 1.2 length. Error bands correspond to +/- 1 *SEM.* **B**: Fast Fourier Transform (FFT) amplitude spectra of mean absolute error across delay periods for the DSR (red) and NEU (blue) tasks. Solid lines represent group-averaged amplitudes (in degrees of error). Dashed lines show statistical significance thresholds (95th percentile) derived from permutation testing. * symbols indicate peaks surviving Bonferroni-correction for number of peaks exceeding statistical threshold. **C.** Polar plots depicting phase angles at the dominant oscillatory frequency in the DSR task (15.00 Hz; left) and the NEU task (20.62 Hz; right). Individual participants are shown as dots at unit radius. The black line represents the mean resultant vector, with its length corresponding to the Phase Locking Value (PLV) and direction indicating the mean phase angle. * denotes significant PLV.

Between-subject phase alignment was quantified for the dominant frequency of each task. In the DSR task, participants exhibited phase locking of performance fluctuations at 15 Hz (Phase Locking Value [PLV] = 0.628, permutation p = 0.0008). In the NEU task, between-subject phase alignment was not significant at 20 Hz (PLV = 0.383, permutation p = 0.095). Rayleigh tests for non-uniformity confirmed these findings (DSR: z = 6.31, p = 0.001; NEU: z = 2.34, p = 0.095; **Fig. 3B**). To test whether between-subject phase alignment differed between the tasks, we conducted permutation tests comparing PLVs. When comparing each task at its dominant frequency (DSR at 15 Hz vs. NEU at 20.62 Hz), we found that the PLV difference was not significant (ΔPLV = 0.245, p = 0.33). Thus, while DSR exhibited significant between-subject phase alignment at 15 Hz and NEU did not at 20.62 Hz, the magnitude of phase locking did not differ reliably between tasks.

When we applied the FFT analysis to inter-item bias, no significant oscillatory peaks were observed in either task (all p > 0.05), indicating that, unlike MAE, inter-item bias did not vary rhythmically (**Supplementary Figure 3**).

Interim discussion—Experiment 1

The results from Experiment 1 provided support for three effects of prioritization on working memory. First, prioritization in the DSR task was associated with a reduction in inter-item interference at recall: The biasing influence of *Sample 2* on the recall of *Sample 1* was markedly reduced. Furthermore, although small biases were present at some angular separations, a critical difference from the NEU task was that these biases were uniform across separation magnitudes, whereas for NEU attraction was strong when items were similar and reduced when items were dissimilar. This suggests that

prioritization has a general effect of attenuating inter-item interference, reducing sensitivity to the similarity between items. Second, prioritization altered the effect of presentation order on recall accuracy. In NEU, recall was more accurate for the more recently presented item (*Sample 2*), consistent with recency advantages observed in prior multi-item working memory studies (Vergauwe et al., 2016; Pomper & Ansorge, 2021; Chota et al., 2022). In DSR, in contrast, this pattern was reversed: when *Sample 1* was prioritized, it was recalled more accurately than when *Sample 2* was prioritized. This suggests that prioritization is particularly effective for the earlier-presented item, whose representational strength is otherwise diminished by subsequently-presented items. Third, prioritization in the DSR task was associated with a lower frequency of behavioral oscillation of mean absolute error (15 Hz; “low-beta”) relative to the NEU task (20 Hz; “higher-beta”). Furthermore, only in DSR was the cue associated with phase-locking of the behavioral oscillation across participants (although this effect did not differ significantly between the two tasks). Coupled with the absence of evidence of rhythmic modulation of the strength of inter-item bias, these results suggest that behavioral oscillations of MAE reflect fluctuations in representational strength rather than periodic distortions in the remembered content. This evidence for behavioral oscillations in the beta band is of particular interest in light of previous work demonstrating an important role for beta-band dynamics in the encoding of priority in working memory (Rose et al., 2016; Fulvio et al., 2024; Fulvio & Postle, 2025).

Rhythmicity is a prominent feature of neural systems supporting visual attention (Buschman & Miller, 2009; Fiebelkorn & Kastner, 2019) and visual working memory (Lundqvist et al., 2016; Bastos et al., 2018; Abdalaziz et al., 2023). One longstanding

and influential perspective holds that, when multiple items are held in working memory, the encoding of individual items at different phases of a low-frequency oscillation provides a mechanism for individuating items and minimizing interference between them (e.g., Siegel et al., 2009; Abdalaziz et al., 2023), and may even be a basis for understanding capacity limitations (Lisman & Idart, 1995; Hakim & Vogel, 2018). For human visual working memory, one study recording the electroencephalogram (EEG) while subjects held two items in mind has identified evidence for phase coding in the beta band (albeit at a higher frequency than the low-beta and higher-beta that we observed in Experiment 1; Abdalaziz et al., 2023). Thus, one prediction that we planned to test in Experiment 2 was that phase encoding of stimulus information in the low-beta band may be a mechanism underlying the shielding effect of prioritization.

The idea of phase encoding in the beta band (c.f., Abdalaziz et al., 2023), together with Experiment 1's evidence for beta-clocked behavioral oscillations, raise an important question about EEG dynamics observed during working memory: To what extent is this activity reflective of one or more truly periodic processes versus activity that, when assessed at the level of the single trial, is fundamentally bursty. In skeletomotor control, "beta bursts" have a prominent role in stopping the execution of motor actions and, by analogy, this phenomenon has been proposed as a mechanism for imposing inhibitory control across many domains of high-level cognition, including long-term memory, visual attention, visual working memory, and language processing (Lundqvist et al., 2024; Wessel & Anderson, 2024). Empirically, reanalysis of a dataset originally interpreted as showing sustained, load-dependent activity in the alpha and beta bands during the delay period of a working memory task has revealed that, at the

single-trial level, this activity was driven by oscillatory bursts (Kavanaugh et al., 2026). Despite these considerations, however, it is difficult for us to conceive of how a relatively sparse, stochastic, and bursty phenomenon could underlie a behavioral oscillation derived from a time series that was assembled via the after-the-fact sorting of trials in order of duration. Nonetheless, another important question for Experiment 2 was to assess whether, at the single-trial level, activity in the low-beta and higher-beta frequency bands of the EEG would more closely resemble persistent oscillating signals or stochastic bursting.

Experiment 2

Materials & methods

Participants

A separate sample of 16 neurologically healthy members of the University of Wisconsin–Madison community (10 females, 21-28 years, *M* = 23.7 years) participated in the EEG experiment, and all data were used in the final analyses. The sample size was chosen to match the sample size of Experiment 1. All participants had normal or corrected-to-normal vision, and all reported having normal color vision. The research was approved by the University of Wisconsin—Madison Health Sciences Institutional Review Board. All participants gave written informed consent at the start of the session and received monetary compensation in exchange for participation.

Experimental stimuli, procedure, and design

The experimental stimuli, procedure, and design were the same as those of Experiment 1, other than the following differences: (i.) *Delay 1.2* of both tasks had a

fixed length of 4 s. (ii.) Participants completed four blocks of the DSR task followed by two blocks of the NEU task, with each block consisting of 60 trials. (iii.) A full-factorial design was ensured whereby each inter-item angular difference magnitude was selected for 30 trials, with each base orientation being selected for 5 of those 30 trials yielding 120 total trials of the NEU task. For the DSR task, we doubled the trials to accommodate the 'stay'/'switch' aspect of the task, yielding 240 total DSR task trials.

EEG recording and preprocessing

EEG was recorded from 63 electrodes with a BrainVision Recorder using active Ag/AgCl electrodes feeding into an ActiCHamp amplifier (BrainProdcuts GmbH). The electrodes were positioned according to the extended International 10–20 system. Impedances were kept below 25 kΩ, and the data were sampled at 1000 Hz. An electrode placed on the forehead served as ground, and all channels were referenced online to channel Fpz and re-referenced offline to the average of all electrodes.

Data were processed offline using EEGLAB (Delorme & Makeig, 2004) with the FieldTrip toolbox (Oostenveld et al., 2011), and custom MATLAB scripts. The data were downsampled to 500 Hz and were bandpass filtered between 1 and 100 Hz with a notch filter centered at 60 Hz. Electrodes exhibiting excessive noise were removed and re-referenced to the average of all remaining electrodes. The continuous data were then epoched to 500 ms prior to *Sample 1* through the feedback in the NEU task, and through the second feedback in the DSR task. Automatic artifact epoch detection and rejection were then performed using the EEGLAB *pop_autorej.m* procedure. The data then underwent dimensionality reduction to 32 principal components, upon which an independent component analysis was applied to identify and remove components

containing eye movement artifacts and muscle artifacts using ICLabel (Pion-Tonachini et al., 2019). Finally, electrodes with excessive noise were interpolated using the spherical spline method.

Behavioral analyses

We carried out analyses of the mean absolute error of recall and of inter-item bias according to the procedures described in the corresponding sections of the Methods of Experiment 1. Mirroring the reported results of Experiment 1, mean absolute error and grand linear mixed effects modeling of inter-item biases are reported below; see **Supplementary Figure 5** for separate analyses of inter-item bias due to current and previous trial memory items.

EEG spectral analysis

Broadband oscillatory peak extraction. For both tasks, we isolated oscillatory peaks from *Delay 1.1* and *Delay 1.2* (i.e., the epoch preceding the cue and following the cue), excluding the first 100 ms of both to minimize visual stimulus-related effects. Because *Delay 1.1* was 500 ms in length, this yielded a window of 400 ms from which to extract oscillatory peaks. To match this, analyses of *Delay 1.2* were restricted to a 400 msec-long window that began 100 msec after the offset of the cue. We computed the power spectral density for each epoch using multitaper Fast Fourier Transform (mtmfft) with Hanning tapering across a frequency range of 3-40 Hz. Spectra were calculated for individual trials and then averaged across trials for each participant.

To isolate oscillatory peaks from the background aperiodic (1/f) component, we applied the Specparam algorithm (formerly FOOOF; Donoghue et al., 2020) with the following parameters: 3-40 Hz frequency range; 5-12 Hz peak width limits; 4 peaks per

channel maximum; 0.15 minimum peak height; 2.0 peak threshold; fixed aperiodic mode. For each channel, the algorithm fitted the aperiodic component and identified oscillatory peaks. For visualization, we plotted histograms of all identified peaks across participants and channels for each task and delay period. We used two-sample Kolmogorov-Smirnov (K-S) Tests to assess whether the distributions of peak frequencies differed between epochs. Because the K-S test is sensitive to any differences in distribution shape, location, or spread, and detects the largest local discrepancy between distributions, significant results would indicate that there were global distributional changes in oscillatory peak frequencies between epochs. To test for differences in central tendency (median) between the distribution of peaks from the two epochs (i.e., *Delay 1.1* vs. *Delay 1.2*), we used Mann-Whitney U tests, for which significant results would indicate that there were systematic shifts in the peak median frequency between epochs. Finally, we calculated the Wasserstein distance (Earth Mover's Distance) between the distributions of peaks from the two epochs. This measure quantifies the minimum cost of transforming one distribution into the other, computed across the *entire* frequency distribution, accounting for both the magnitude of differences and the distance over which spectral energy must be displaced (Rubner et al., 2000; Lipp & Vermeesch, 2023). The Wasserstein distance was calculated for the pooled data (i.e., all peaks extracted across participants) between all peak frequencies from *Delay 1.1* and all peak frequencies from *Delay 1.2* using 200 quantile comparison points. We then shuffled the epoch labels and computed the distance 5,000 times and the *p*-value was computed as the proportion of shuffled data sets that showed a distance equal to or greater than the actual observed distance. We also performed a

participant-level analysis, computing the distance between epochs for each participant, then shuffling the condition labels within that participant's data set 2,000 times to create a participant-specific null distribution. To assess whether within-participant distributional shifts were consistent across participants, we randomly sampled one value from each participant's null distribution and averaged across participants (repeated 2,000 times), and compared the observed group mean distance to this null distribution.

Beta band peak extraction. We next refined our peak extraction analysis by focusing on the two ranges identified in the MAE behavioral oscillations in Experiment 1: a 'low-beta' range of 14-16 Hz; and a 'higher-beta' range of 19-21 Hz. The spectral analysis pipeline used for broadband peak extraction was applied to the same *Delay 1.1* and *Delay 1.2* epoch data from the DSR and NEU tasks, extracting peaks only in the specified low-beta and higher-beta ranges. For each channel and participant, we extracted all peaks in each band and averaged the band counts separately across channels. We then used a three-way repeated measures ANOVA with factors: Task (DSR vs. NEU), Band (low-beta: 14-16 Hz vs. higher-beta: 19-21 Hz), and Epoch (*Delay 1.1* vs. *Delay 1.2*) to quantify differences in beta peak density (in units of peaks per channel). Follow-up analyses included task-specific paired *t*-tests comparing peak densities across epochs within each band and a focused test of the Band × Epoch crossover pattern identified in the DSR condition. For visualization, we plotted the group-average beta peak density topographically across conditions. These topographic maps are descriptive and were not subject to statistical testing due to sparse peak distributions.

Aperiodic component analysis. In addition to analyzing oscillatory peaks, we examined the aperiodic component of the power spectra, which reflects broadband neural activity independent of narrowband oscillations. The Specparam algorithm models the aperiodic component as a 1/f-like function characterized by two parameters: the offset (reflecting broadband power) and the exponent (reflecting the slope of the power spectral decay, which has been proposed as a proxy for the balance between neural excitation and inhibition ("E:I balance"; Gao et al., 2017; Waschke et al., 2021). For each participant, we extracted the aperiodic exponent and offset for each channel, then averaged across channels to obtain a single value per participant for each epoch and task. To test whether aperiodic parameters changed across delay periods, and whether these changes differed by task, we conducted 2 (Task: DSR, NEU) × 2 (Epoch: *Delay 1.1*, *Delay 1.2*) repeated measures ANOVAs separately for offset and exponent. Prior to analysis, we assessed normality of the difference scores using the Lilliefors and Anderson-Darling tests. Because the exponent difference scores violated normality assumptions in the DSR task (Lilliefors p = .005, kurtosis = 5.35), we supplemented the parametric ANOVAs with non-parametric Wilcoxon signed-rank tests on the epoch effects collapsed across tasks.

Sub-band burst rate analysis. To examine frequency-specific temporal dynamics of beta bursts, we separately quantified burst rates in the low-beta (14-16 Hz) and higher-beta (19-21 Hz) frequency bands. Bursts were detected using the Matlab implementation of the SpectralEvents toolbox (https://github.com/jonescompneurolab/SpectralEvents) with time-frequency analysis conducted via Morlet wavelet decomposition (width = 5) across 13-30 Hz. Following

prior studies, findMethod = 1 was used as in Shin et al., 2017, see also Kavanaugh et al., 2026, which is agnostic to event overlap, and an event threshold of 6× the median power across time and epochs for each frequency bin of the time-frequency representation.

For each participant, bursts with a peak frequency falling within each sub-band of interest were identified, and their rates (events per second) were calculated for the same two temporal epochs used in the oscillatory peak analysis (see ***Broadband oscillatory peak extraction***): the final 400 ms of *Delay 1.1* (pre-cue baseline period) and a 400 ms window beginning 100 ms after cue onset during *Delay 1.2* (post-cue period). Burst rates were averaged across all scalp electrodes to yield a single value per participant, task, epoch, and frequency band.

We first computed two descriptive measures of trial prevalence to characterize burst prevalence. First, we calculated the proportion of trials containing at least one burst within each channel, then averaged these proportions across channels (per-channel prevalence). Second, we calculated the proportion of trials containing at least one burst anywhere across all channels (any-channel prevalence), which provides a more direct estimate of how frequently bursts occurred during the epochs.

Statistical analyses utilized paired *t*-tests comparing low-beta and higher-beta burst *rates* (events/sec) within each task and epoch, paired *t*-tests comparing *Delay 1.1* and *Delay 1.*2 burst rates within each frequency band and task, and separate 2×2 repeated-measures ANOVAs (Task [DSR vs NEU] × Epoch [*Delay 1.1* vs *Delay 1.2*]) for each frequency band to assess main effects and interactions.

Oscillatory power. To complement the spectral parameterization and burst rate analyses, we examined oscillatory power in the low-beta (14-16 Hz) and higher-beta (19-21 Hz) frequency bands. Time-frequency decomposition was performed using Morlet wavelets (width = 5 cycles) as implemented in FieldTrip. Power was computed over the timepoints spanning *Delay 1.1* through *Delay 1.2* (a total of 5000 ms sampled at 250 Hz for 1250 timepoints) in 50 ms steps. We decomposed power into induced and evoked components. Total power was computed by first applying wavelet decomposition to each trial and then averaging across trials. Evoked power was computed by first averaging the raw signal across trials to obtain the event-related potential and then applying wavelet decomposition to the averaged signal. Induced power was calculated as total power minus evoked power, isolating oscillatory activity that was not phase-locked to stimulus onset.

Initially, the power values were not baseline-corrected because the period preceding *Delay 1.1* contained stimulus presentation (*Sample 2*) and thus did not provide an appropriate baseline. For statistical analysis, power was averaged across all channels and across the two time windows used in the other spectral analyses described above: the final 400 ms of *Delay 1.1* and the first 400 ms of *Delay 1.2*, offset by 100 ms to avoid sample-evoked and cue-evoked transients, respectively. Induced and evoked power were analyzed separately for each frequency band using 2 × 2 repeated measures ANOVAs with factors Task (DSR, NEU) and Epoch (pre-cue, post-cue). Follow-up paired *t*-tests were carried out to examine simple effects the two factors with a Bonferroni-corrected alpha-level = .025 (for two comparisons per effect/band).

Because strong task differences emerged in the non-baseline-corrected analysis, we carried out a follow-up comparison of the power in the two tasks using *Delay 1.1* as the baseline allowing us to address whether the power in the two tasks exhibited differential cue-related changes in power, rather than just differing in absolute power levels. For each participant, we computed the percent change in power from pre-cue to post-cue as ((*post* − *pre*) / *pre*) × 100 separately for each frequency band and power type (induced, evoked). Paired *t*-tests were carried out to test for differences in percent power change between DSR and NEU at the Bonferroni-correct alpha-level = .025.

Time-resolved representational similarity analysis (RSA)

To examine how neural representations of prioritized and unprioritized memory items (i.e., PMIs and UMIs) evolved over time, we computed a time-resolved representational similarity analysis (RSA) separately for each item and participant. After the preprocessed EEG data were downsampled to 250 Hz and baseline-corrected by subtracting each channel's trial-averaged activity, for each participant, and timepoint, we constructed representational dissimilarity matrices (RDMs) capturing the pairwise dissimilarities (1 − Pearson's *r*) between condition-averaged ERP patterns across electrodes. Conditions were defined by all 24 combinations of angular difference (0°, +/-22.5°, +/-45°, +/-67.5°) and base orientation (10°–160° in 30° steps), separately for PMIs and UMIs in the DSR task. If there were no trials for a particular combination of angular difference + base orientation in a priority condition (due to the removal of bad trials during pre-processing), that row and column were omitted from the analysis. This occurred for 1 row/column of 1 participant's analysis. Because the NEU task had half the number of trials as the DSR task, row/column omissions were more frequent for the

tested and untested trial splits, and, as such, conditions were instead defined by the 6 base orientations, collapsing over the four angular difference conditions to ensure more balance across participants. To track representational changes with priority, we first generated two reference models for each task (one each corresponding to the PMI/tested item and to the UMI/untested item) by computing an RDM from the 500 msec of Delay 1.1. Next, RDMs were computed at each timepoint spanning *Delay 1.1* through *Delay 1.2* (in 7-sample (28 ms) windows) and correlated (Spearman's rho) with the reference RDM. The resulting similarity values (i.e., the Spearman correlations) were averaged across participants to produce group-averaged time-resolved representational similarity time courses. Statistical comparisons of group-level representational similarity across epochs (i.e., *Delay 1.1, Cue 1, Delay 1.*2) used paired-sample *t*-tests on the within-participant averaged similarities within the epoch intervals (i.e., similarities were averaged across the 28 ms windows falling within each epoch).

To reveal the importance (contribution) of each electrode's activity to the representation at any point in the analysis interval, we repeated the procedure for the original RSA analysis but for each electrode separately. In this iterative analysis, the reference RDMs were computed as in the original analysis using data from all electrodes during *Delay 1.1*. The timepoint-by-timepoint RDMs, however, only used data from the single electrode being analyzed in the iteration. This analysis thus yielded a similarity map across the scalp, such that electrodes with larger correlations were those with greater importance/contribution to the representational similarity observed at each timepoint in the original analysis. For visualization, the resulting importance maps were

averaged across participants to produce topographic maps of representational similarity during the *Delay 1.1*, *Cue 1,* and *Delay 1.2* epochs.

Spectral analysis of RSA time courses

To characterize rhythmic fluctuations in representational similarity, we spectrally decomposed the RSA time courses. First, each participant's PMI, UMI, tested, and untested RSA time course was mean-centered. Subsequently, the spectral analysis of the RSA was identical to the spectral analysis of the raw EEG (see section ***EEG spectral analysis***), with the following exceptions: (1) Power spectral density was computed using a standard FFT with an NFFT of 512 samples rather than multitaper estimation with Hanning tapering. This is because the RSA time series represents a single derived measure per participant rather than noisy multi-channel electrophysiological recordings, which reduces the need for variance-bias tradeoffs afforded by multitaper methods. (2) Because RSA yields a single time series per participant (rather than multiple channels), peak counts reflect the number of peaks detected in each participant's RSA trace, and aperiodic parameters were extracted directly from each participant's spectrum without averaging across channels.

For the beta band peak extraction analysis, we computed peak counts separately for the PMI and UMI in the RSA time courses in the DSR task, and for the tested and untested items in the RSA time courses in the NEU task. To parallel the task-level EEG analysis, we summed peak counts across PMI and UMI (for DSR) or across tested and untested items (for NEU) before conducting the 3-way repeated measures ANOVA (Task × Band × Epoch). We additionally conducted a 4-way repeated measures ANOVA

including Priority (PMI/UMI or tested/untested) as a factor to examine whether spectral signatures differed by memory item status.

To directly test whether a task-specific beta band dissociation emerged following the retrocue, we conducted a focused analysis of *Delay 1.2* using a 2 (Task: DSR, NEU) × 2 (Band: low-beta, high-beta) repeated measures ANOVA. We followed up significant interactions with simple effects tests comparing tasks within each band, and a crossover test quantifying the difference of task effects across bands (i.e., $[\text{DSR} - \text{NEU}]_{\text{low-beta}} - [\text{DSR} - \text{NEU}]_{\text{higher-beta}}$). We also examined Task × Epoch interactions separately for each band to determine whether cue-related changes in peak counts were task-specific.

For the aperiodic component analysis, we computed 2 (Task) × 2 (Epoch) repeated measures ANOVAs for exponent and offset at the task level (averaging across PMI/UMI or tested/untested), as well as 3-way ANOVAs (Task × Priority × Epoch) to examine priority-specific effects.

To test for evidence of phase encoding of the representations of the two memory items we computed cross-spectral phase consistency between the time-resolved RSA time courses for each item pair (PMI/UMI in DSR; tested/untested in NEU). For each participant, we computed cross-spectral phase using the fast Fourier transform (FFT) with zero-padding to 512 points for the *Delay 1.1* and *Delay 1.2* epochs used in the beta peak extraction analysis and computed the phase difference between the two RSA traces from the angle of the cross-spectrum. Phase values were averaged across frequency bins within the two bands of interest: low-beta (14–16 Hz; 5 bins: 14.16, 14.65, 15.14, 15.62, 16.11 Hz–note that the addition of the final 16.11 Hz bin ensured the complete 2 Hz band would be captured) and higher-beta (19–21 Hz; 5 bins: 19.04,

19.53, 20.02, 20.51, 21.00 Hz), using circular averaging. To assess whether the phase relationships were consistent across participants, we computed the resultant vector length (r) and tested for non-uniformity using the Rayleigh test. We obtained bootstrapped standard errors for r by resampling participants with replacement (5,000 iterations). To test whether cue-related changes in phase consistency differed between tasks, we conducted a permutation test on the Task × Epoch interaction ($r_{DSRpost} - r_{DSRpre}$) − ($r_{NEUpost} - r_{NEUpre}$). The null distribution was generated by independently shuffling epoch labels (pre/post) within each task for each participant (10,000 permutations), and a two-tailed p-value was computed as the proportion of permuted interaction values with absolute magnitude greater than or equal to the observed value.

Results

Behavioral performance

Recall accuracy. Overall levels of mean absolute error (MAE) of recall were comparable to what was observed in Experiment 1: MAE did not differ statistically between DSR *Recall 1* and NEU recall ($t(15) = -2.0024$, $p = .064$), nor for DSR *Recall 2* versus NEU recall ($t(15) = 2.3483$, $p = .033$ (Bonferroni-corrected $\alpha = .0167$); **Fig. 4A**). DSR *Recall 1* was superior to DSR *Recall 2* ($t(15) = 4.7537$, $p < .001$), and 'stay' and 'switch' trials from DSR *Recall 2* did not differ ($t(15) = -1.5845$, $p = .134$; **Supplementary Figure 5**). A linear mixed effects (LME) model confirmed that larger inter-item angular differences were associated with larger absolute errors (main effect: $F(1,189) = 57.837$, $p < .001$; **Fig. 4B**).

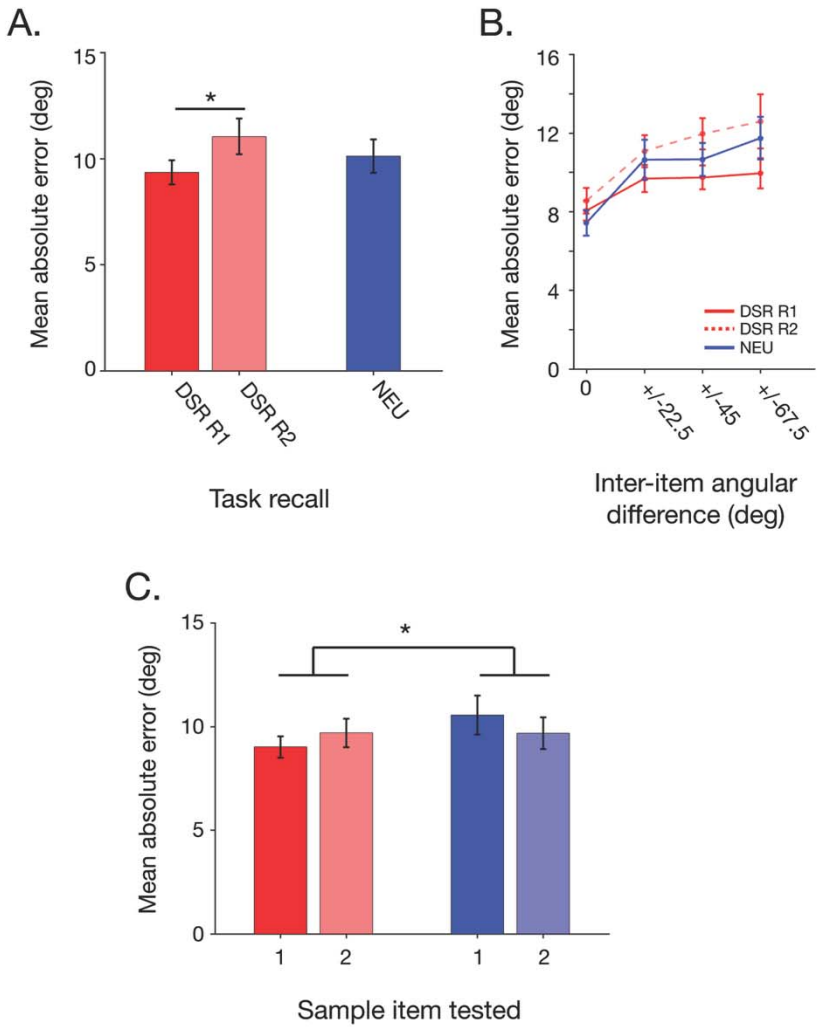

Fig 4. Experiment 2 recall performance. A. Mean absolute recall error for the two responses of the DSR task and the single response of the NEU task. **B.** Same as **A.** separated by the current trial's inter-item angular difference. **C.** Mean absolute error for DSR *Recall 1* and NEU recall as a function of which sample item was tested. Error bars correspond to +/- 1 *SEM.* * symbols correspond to significant differences between conditions at the Bonferroni-corrected alpha level = .0167 for 3 paired-sample *t*-tests (**A.**) and the Bonferroni-corrected alpha level = .025 for two paired-sample *t*-tests and for interaction $p < .05$ (**C.**).

Assessment of MAE as a function of the presentation order indicated that, for NEU, MAE was numerically larger when *Sample 1* was tested ($t(15) = 1.204$, $p = .247$), for DSR, MAE was numerically smaller when was tested ($t(15) = -1.593$, $p = .132$; **Fig. 4C**), and the crossover interaction between the two was significant ($t(15) = -2.276$, $p = .038$).

Across- and within-trial bias. Linear mixed effects modeling indicated that the previous trial's tested item exerted a significant attractive bias on the current trial (NEU: $\beta = 1.60°$, $p < .001$; DSR: $\beta = 0.63°$, $p = 0.04$; **Supplementary Table 5**), an effect that was larger in the NEU task ($\beta = 0.97°$, $p = .032$; **Supplementary Table 6**). The previous trial's untested item had no significant effect on recall in either task. Within-trial effects were dependent on the order of presentation. The recall of *Sample 1* was attracted toward the value of *Sample 2* for NEU ($\beta = 4.10°$, $p < .001$), but not for DSR ($\beta = -0.39°$, $p = .364$), whereas recall of *Sample 2* showed no bias from *Sample 1* in NEU ($\beta = -0.72°$, $p = .131$) but a significant repulsive bias in DSR ($\beta = -1.52°$, $p < .001$; **Supplementary Table 5**). The three-way interaction between task, current untested item, and order-of-presentation was significant ($\beta = -3.67°$, $p < .001$; **Supplementary Table 6**).

Linear mixed effects modeling further revealed that in the NEU task, the effect of inter-item angular difference on bias was marginal ($F(2,2828) = 2.57$, $p = .077$; **Supplementary Table 7**), but inter-item angular difference significantly interacted with order of presentation in recall bias ($F(2,2828) = 3.94$, $p = .019$). Recall of *Sample 1* was significantly attracted toward *Sample 2* at all angular separations (22.5°: 4.56°, $p < .001$; 45°: 3.21° $p < .001$; 67.5°: 2.30° $p = .002$) with a significant reduction at the largest

angular separation (β = -2.26°, p = .025). Recall of *Sample 2,* in contrast, exhibited significant repulsion from *Sample 1* at the small angular separation (22.5°: -1.72° p = .021) but no significant bias at medium and large angular separations (45°: 0.01° p = .986; 67.5°: -0.20° p = .809; main effect of presentation order: $F(1,2828) = 37.99$, $p < .001$).

In the DSR task, there was a significant main effect of presentation order ($F(1,2827) = 6.74$, p = .009) and a significant interaction between presentation order and inter-item angular difference ($F(2,2827) = 4.67$, p = .009). Recall of *Sample 1* showed no significant bias relative to *Sample 2* at any angular separation (22.5°: -0.01° p = .992; 45°: -0.40° p = .535; 67.5°: -0.57° p = .387). Recall of *Sample 2,* in contrast, was significantly repulsed from *Sample 1* at small and medium angular separations (22.5°: -2.33° $p < .001$; 45°: -2.03° p = .001) but no bias at large separations (67.5°: 0.75° p = .220; interaction: β = 3.64°, p = .004).

The previous trial's target did not significantly influence signed bias in either task (DSR: p = .288; NEU: p = .157). The task comparison model confirmed that NEU showed significantly greater overall bias than DSR ($F(1,5657) = 24.49$, $p < .001$), and that the effect of presentation order on bias differed significantly between the tasks (interaction: $F(1,5657) = 8.22$, p = .004; **Supplementary Table 8**): in NEU, presenting the untested item first eliminated attraction, whereas in DSR, it induced repulsion. The effect of inter-item angular difference did not differ significantly between tasks (interaction: $F(2,5657) = 0.69$, p = .502).

In most regards, these results replicated the pattern from Experiment 1 that prioritization shielded the cued item from the influence of other stimuli. In particular, the

attractive bias toward the previous trial and the attractive bias of *Sample 2* on recall of *Sample 1* were markedly smaller in DSR than in NEU. The angular difference analysis further revealed that, as in Experiment 1, the previous trial's target did not influence signed bias, confirming that between-trial and within-trial sources of recall bias operate independently. However, several other findings diverged from Experiment 1. First, recall of *Sample 2* showed greater repulsion from *Sample 1* in DSR vs. NEU. Second, for DSR, recall of *Sample 2* showed repulsion from *Sample 1* for angular separations of 22.5° and 45°. Third, for NEU, recall of *Sample 1* showed a uniform pattern of attraction across angular separations and a significant repulsion of *Sample 2* from *Sample 1* for angular separations of 22.5°. We will discuss these effects in Interim Discussion—Experiment 2.

EEG spectral analysis

Oscillatory components. For the DSR task, visual inspection of the full distribution of extracted peak frequencies pooled across all participants and channels revealed a post-cue increase in the number of peaks in the low-beta range (**Fig. 5A**), an effect confirmed by K-S test (D = .1367, p < .001). A follow-up Mann–Whitney U test found that the difference identified by the K-S test was not due to a shift in central tendency (z = 1.13, p = .260), indicating that the effect reflected differences in distributional shape. This was confirmed by a permutation test on Wasserstein distance between the two pooled distributions, which was significant (mean distance = 1.22 Hz, permutation p < .001). To assess whether these pooled differences were consistent across participants, we computed the Wasserstein distance between each participant's peak distributions in the two epochs. Participants consistently exhibited significant non-

zero within-subject distributional differences (mean distance = 2.59 Hz; permutation $p < .001$).

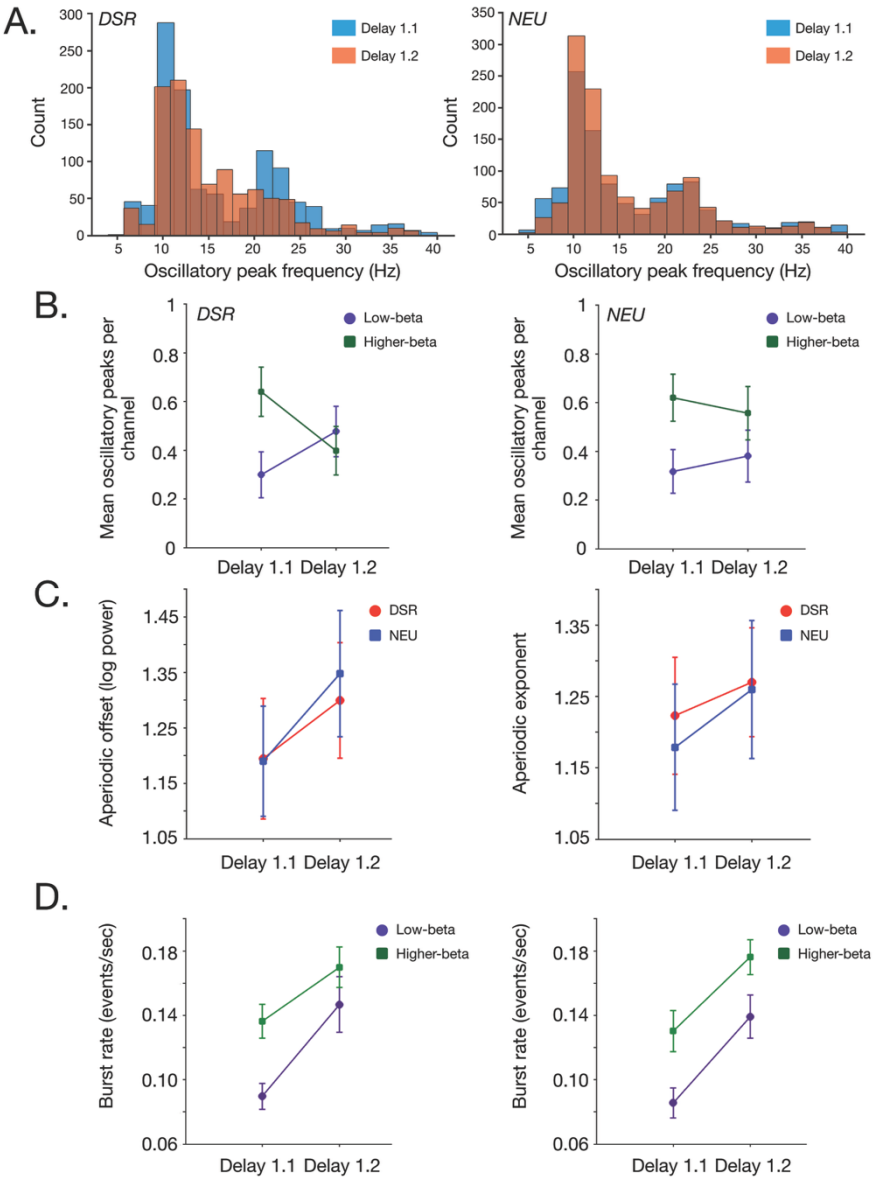

Fig 5. EEG spectral properties. A. Distribution of all oscillatory peak frequencies identified across channels and participants from *Delay 1.1* (light blue) and *Delay 1.2* (orange) for the DSR task (left) and for the NEU task (right). **B.** Group-averaged mean number of low beta peaks (indigo circles) and higher-beta peaks (green squares) per channel from *Delay 1.1* and *Delay 1.2* for the DSR task (left) and the NEU task (right). **C.** Left: Mean aperiodic offset for *Delay 1.1* and *Delay 1.2* in the DSR task (red circles) and in the NEU task (blue squares). Right: Mean aperiodic exponent for *Delay 1.1* and *Delay 1.2* in the DSR task (red circles) and in the NEU task (blue squares). **D.** Group-averaged mean low-beta burst rate (indigo circles) and higher-beta burst rate (green squares) per channel from *Delay 1.1* data and *Delay 1.2* data for the DSR task (left) and the NEU task (right). Error bars correspond to +/- 1 *SEM.*

Results for the NEU task differed from DSR: the cue-locked change of the full distributions of peak frequencies was a shift toward a greater number of peaks in the alpha frequency range (**Fig. 5A**), an effect confirmed by K-S test (D = .0623, p = .024), with no change in median peak frequency (z = 0.1675, p = .867). At the group level, participants consistently exhibited non-zero Wasserstein distances between epochs (mean distance = 2.31 Hz; permutation p < .001), indicating that the distributions of peaks in the NEU task also changed in a consistent manner across participants, despite no shift in central tendency.

We next focused our analysis on detection of oscillatory peaks in the two sub-bands identified in the analysis of behavioral oscillations of Experiment 1: 14-16 Hz ('low-beta') and 19-21 Hz ('higher-beta'). Visual inspection of the results suggested an interaction between task and epoch in the number of low-beta vs. higher-beta peaks extracted (**Fig. 5B**). A three-way repeated measures ANOVA did not find a significant three-way Beta band × Task × Epoch interaction (F(1,15) = 0.8873, p = .361). However, a more focused analysis revealed task-specific patterns. In the DSR task, there was a significant crossover pattern whereby the number of low-beta and higher-beta peaks changed in opposite directions across the delay epochs (t(15) = 2.3586, p = 0.032), with higher-beta decreasing significantly from *Delay 1.1* to *Delay 1.2* (mean change = -0.242 peaks/channel, t(15) = -2.41, p = 0.029); an effect most prominent at frontal and occipital electrodes (**Supplementary Figure 6**) and low-beta showing a numeric increase (mean change = 0.178 peaks/channel, t(15) = 2.02, p = 0.061); a trend most prominent at occipital and parietal electrodes (**Supplementary Figure 7**). The NEU condition, in contrast, showed stable patterns in these two sub-bands across the two

epochs (all p-values > 0.6).

Aperiodic spectral component. For the aperiodic offset, the ANOVA revealed a significant main effect of Epoch, ($F(1,15) = 11.07$, $p = .005$), with offset increasing from *Delay 1.1* ($M = 1.19$) to *Delay 1.2* ($M = 1.32$). This indicated elevated broadband power during the post-cue portion of the delay period. There was no main effect of Task ($F(1,15) = 0.23$, $p = .64$) and no Task × Epoch interaction ($F(1,15) = 3.56$, $p = .08$; **Fig. 5C**). For the aperiodic exponent, spectral slopes were numerically steeper during *Delay 1.2* versus *Delay 1.1*, ($F(1,15) = 3.63$, $p = .076$), with no effect of Task ($F(1,15) = 0.58$, $p = .46$), and no interaction ($F(1,15) = 2.39$, $p = .14$). Non-parametric tests collapsing across tasks confirmed significant epoch effects for both offset (Wilcoxon signed-rank, $z = -2.79$, $p = .005$, $r = .70$) and exponent ($z = -2.22$, $p = .026$, $r = .56$).

***Burst analysis*.** Many analyses of intra- and extracranial recordings have shown that beta-band effects observed in trial-averaged electrophysiological data can be shown to be due to bursting—rather than to a sustained oscillating signal—at the single-trial level. Because the EEG effects relating to the behavioral oscillations from Experiment 1 (**Fig. 5**) emerged from a spectral parameterization routine that is carried out on trial-averaged power spectra, it was important that we assess whether these effects might also be due to bursting in the low-beta and higher-beta frequency bands.

We carried out our burst analyses with routines that had previously been applied to EEG data from a working memory task to demonstrate that averaged power dynamics in the traditionally defined beta band (15-29 Hz) could be accounted for by burst dynamics observed at the single-trial level (Kavanaugh et al., 2026). Thus, to validate our approach, we first applied a burst analysis to the 4 sec epochs of *Delay 1.2*

from the NEU task, from the P3 electrode, bandpass filtered to 15-29 Hz ("broadband beta"). This yielded burst frequencies of NEU: of 0.91 bursts/sec (SD = .13); DSR: 0.89 bursts/sec (SD = .13). These values are similar to the 1.21 bursts/sec (SD = .22) obtained by (Kavanaugh et al., 2026; B.C. Kavanaugh, personal communication). In the narrower "low-beta" (14-16 Hz) and "higher-beta" (19-21 Hz) bands, however, bursts were sparse events that occurred infrequently at any individual electrode (3-7% of trials per channel), although when considering all channels simultaneously, in low-beta, at least one burst occurred on 49.5-65.3% of trials (depending on delay epoch and condition) and in higher-beta, on 66.9-76.3% of trials, with similar prevalences in the two tasks. Despite the rare occurrence of bursts in these two frequency bands, the burst rate in both showed a significant increase from *Delay 1.1* to *Delay 1.2*, albeit with no differences between the DSR and NEU tasks, with values for *Delay 1.1* ranging from 0.086-0.13 bursts/sec and values for Delay 1.2 ranging from 0.139-0.176 events/sec (**Fig. 5D**). Separate repeated-measures ANOVAs (Task × Epoch) for each frequency band confirmed significant main effects of Epoch (low-beta: $F(1,15) = 19.72$, $p < 0.001$; higher-beta: $F(1,15) = 16.66$, $p < 0.001$), with no main effects of Task (both p-values > 0.38) and no Task × Epoch interactions (both p-values > 0.29). Within-task paired t-tests confirmed significant increases from *Delay 1.1* to *Delay 1.2* for both bands in both tasks (all $p \leq 0.004$). Comparing burst rates across frequency bands, higher-beta bursts were more frequent than low-beta bursts during *Delay 1.1* (both tasks: $t(15) > 5.37$, $p < 0.001$), but this difference diminished during *Delay 1.2* (DSR: $t(15) = 2.25$, $p = 0.04$; NEU: $t(15) = 3.45$, $p = 0.004$), reflecting a proportionally larger increase in low-beta burst activity in the early delay period following the cues.

Power. To characterize the phase-locking properties of beta-band activity, we decomposed raw EEG power in the low-beta and higher-beta bands into induced (non-phase-locked) and evoked (phase-locked) components. Across both tasks and both frequency bands, power was almost exclusively induced, with evoked power constituting only ~1-2% of total power (**Supplementary Figure 8**).

Induced power did not mirror the task-specific *Delay 1.1* to *Delay 1.2* crossover pattern observed in the peak extraction analysis (**Supplementary Figure 8A**). In low-beta, there was a main effect of Task ($F(1,15) = 5.79$, $p = .030$), with NEU showing greater induced power than DSR across both epochs, but no Task × Epoch interaction ($F(1,15) = 1.72$, $p = .210$). In higher-beta, there was a main effect of Epoch ($F(1,15) = 9.38$, $p = .008$), with induced power increasing from *Delay 1.1* to *Delay 1.2* in both tasks with no interaction ($F(1,15) = 1.48$, $p = .242$). The absence of interactions indicates that raw power measures—which conflate periodic oscillations with aperiodic activity—do not capture the subtle, task-specific shifts in oscillatory peak distributions revealed by the spectral parameterization. The epoch effect in higher-beta power may reflect the task-general increases in burst rate and aperiodic offset reported above.

Evoked power, which reflects phase-locked oscillatory activity, revealed a different pattern (**Supplementary Figure 8B**). Both frequency bands showed significant main effects of Task (low-beta: $F(1,15) = 7.83$, $p = .014$; higher-beta: $F(1,15) = 20.11$, $p < .001$) and Epoch (low-beta: $F(1,15) = 9.38$, $p = .008$; higher-beta: $F(1,15) = 13.20$, $p = .003$), with no interactions (both p-values > .37). In both bands, NEU evoked power was greater than DSR, particularly during the post-cue epoch. This is consistent with a more stereotyped, phase-consistent neural response to the uninformative cue in the NEU

task, and more variable power timing across trials in response to the retrocue in the DSR task.

Finally, to determine whether task differences reflected differential cue-related modulation rather than baseline differences, we computed percent power change from pre-cue to post-cue using *Delay 1.1* as baseline. Induced power showed no task differences in percent change (low-beta: $t(15) = -1.25$, $p = .23$; higher-beta: $t(15) = -1.22$, $p = .24$; **Supplementary Figure 8C**), indicating that both tasks exhibited similar cue-related increases in non-phase-locked power. By contrast, evoked power revealed a significant task difference in low-beta ($t(15) = -3.46$, $p = .004$): DSR exhibited a larger decrease in phase-locked power (-48.1 ± 8.2%) compared to NEU (-24.9 ± 7.4%). Higher-beta showed a similar numerical pattern but did not reach significance (DSR: -35.0 ± 9.6%; NEU: -19.7 ± 7.5%; $p = .17$). This pattern is consistent with a more disruptive effect of the informative retrocue (DSR) compared to the uninformative cue (NEU) on cross-trial phase consistency.

Interim summary—EEG spectral analysis

Filtering the EEG data into two narrow bands identified in Experiment 1—“low beta” (14-16 Hz) and “higher-beta” (19-21 Hz)—produced results that are broadly congruent with the behavioral oscillations observed in Experiment 1. Specifically, in the DSR task, the prioritization cue triggered a shift toward more prominent oscillatory activity in the low-beta band (together with a shift away from higher-beta). In the NEU task, in contrast, there was only evidence of a shift toward more prominent activity in the alpha band. Analyses of the aperiodic component of the data revealed effects that were common to both tasks. For broadband power (i.e., the offset parameter), there was an increase

from *Delay 1.1* to *Delay 1.2*, consistent with a ramping of neural activity leading up to the response. For spectral slope (i.e., the exponent parameter) there was evidence, albeit weaker, for a steeper slope during *Delay 1.2*, which would be consistent with a shift in E:I balance toward greater relative inhibition. Beta-burst rates, although in the expected range within the classically defined beta band, were too sparse in the two narrow bands of theoretical interest to be candidate substrates of the behavioral oscillations observed in Experiment 1. Nonetheless, consistent with the oscillatory dynamics, burst rates increased from pre-cue to post-cue periods in both the low-beta (14-16 Hz) and higher-beta (19-21 Hz) bands, albeit with no task differences. Finally, raw power measures did not capture the task-specific oscillatory signatures identified through spectral parameterization, although evoked power analyses revealed that the informative retrocue in DSR was more disruptive to cross-trial phase consistency than the uninformative cue in NEU.

Representational similarity

***Time-course analyses*.** In the DSR task, onset of *Cue 1* triggered an abrupt shift in the neural representation of both items (**Fig. 6A**). For the PMI, its representation during both the *Cue 1* and *Delay 1.2* epochs was significantly different from (i.e., less correlated with) the reference RDM (i.e., with its representation during *Delay 1.1;* both *p*-values $\leqq$ .0027). After the initial transformation, the RSA time course was stable, in that the PMI's similarity with respect to the *Delay 1.1* reference RDM did not differ between the *Cue 1* and *Delay 1.2* epochs ($t(14) = 1.7488$, $p = .102$). For the UMI, its representation during the *Cue 1* and *Delay 1.2* epochs was also significantly different

from the *Delay 1.1* reference RDM (both *p*-values $\leqq$ .001). Unlike the PMI, however, the representation of the UMI continued to change after cue offset, such that its correlation with the reference RDM was higher during the *Cue 1* epoch than during the *Delay 1.2* epoch ($t(14) = 3.4866$, $p = .004$). When comparing the two memory items directly, the representational shift of the UMI were more pronounced than those of the PMI: during the *Cue 1* epoch the UMI's representational dissimilarity relative to the *Delay 1.1* reference RDM was greater than that for the PMI ($t(14) = 2.1889$, $p = .046$). This difference persisted through *Delay 1.2* ($t(14) = 2.3878$, $p = .032$).

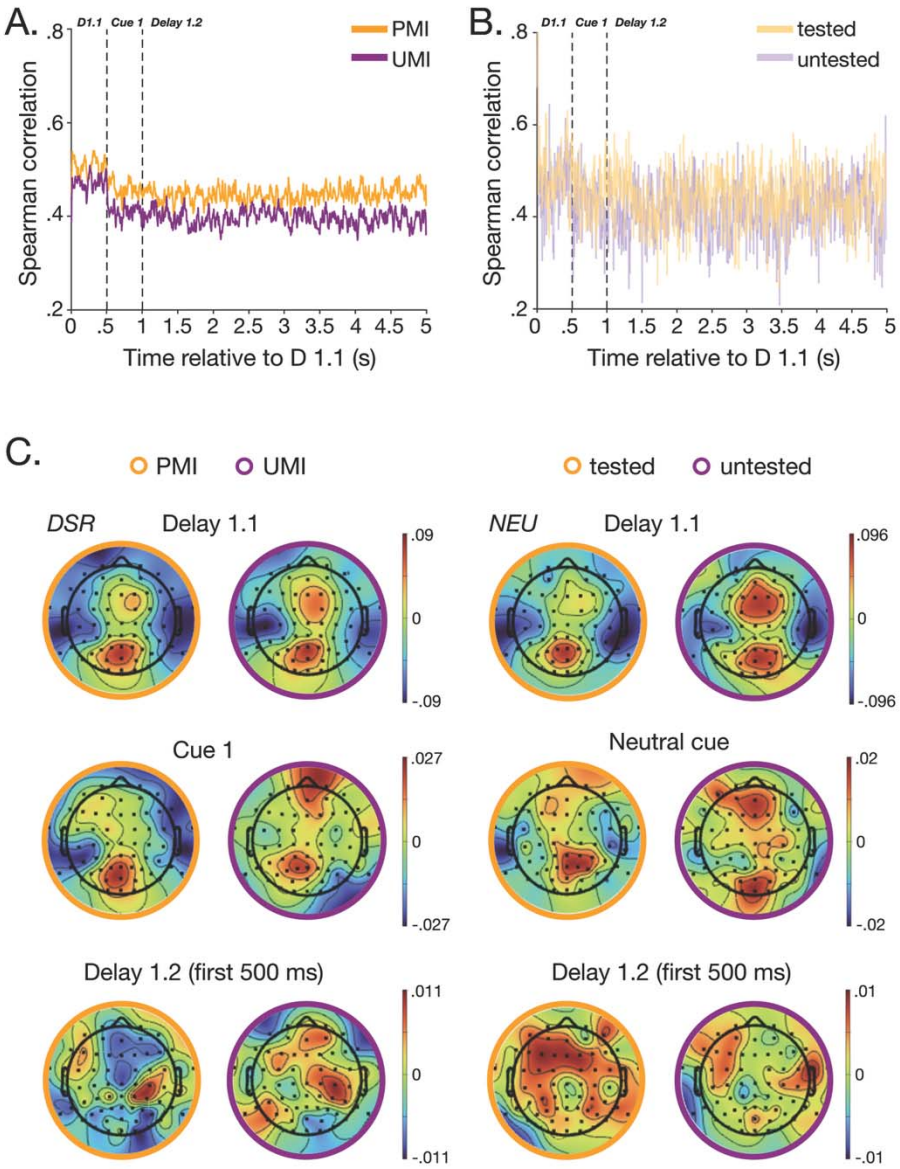

Fig 6. Time-resolved representational similarity. A. Time-resolved similarity traces for the correlation of representation of the PMI (orange) and UMI (purple) at each time point spanning *Delay 1.1* through *Delay 1.2* with the representation of each item over the duration of *Delay 1.1.* **B.** Same as **A.** for the tested (light orange) and untested (light purple) item representations of the NEU task. **C.** Topographic importance maps depicting the relative contributions of each electrode's activity to the RSA traces in panels **A.** and **B.** for the DSR task (right) and NEU task (left), during *Delay 1.1* (top row), cue epochs (middle row), and *Delay 1.2* (bottom row). Warmer colors indicate stronger contribution to the overall similarity estimates.

For the NEU task, variability of the RSA time course was visibly higher than for the DSR task. Although both items exhibited changes in representational similarity across the epochs (all *p*-values < .005), these time courses did not exhibit the abrupt cue-locked transformations observed in the DSR task (**Fig. 6B**). Furthermore, the degree of dissimilarity with respect to the reference RDM did not differ between the two items in any of the epochs that were analyzed (all *p*-values > .596).

Inspection of the topographic importance maps for the RSA reveals similar patterns during *Delay 1.1* for both memory items in both tasks, with prominent contributions from a set of occipital-parietal electrodes and a separate set of frontal-midline electrodes (**Fig. 6C**). These distributions changed only subtly during the cue epoch, then more markedly during *Delay 1.2.* For the DSR task, for the PMI only, a reversal of sign was observed at frontal midline electrodes for *Delay 1.2* versus earlier epochs.

Spectral analyses—beta-band peak extraction at the task level. To assess whether the oscillatory dynamics of neural representations may also show similarities with the behavioral oscillations revealed by Experiment 1, we next quantified oscillatory patterns in the time-resolved RSA data. To do this, we first extracted beta-frequency peaks from the PMI/tested and UMI/untested RSA time courses, separately in the two narrow bands identified in behavioral oscillations (**Fig. 3**): 'low-beta' (14-16 Hz) and 'higher-beta' (19-21 Hz). Next, to enable a direct comparison with the task-level EEG spectral analysis (**Fig. 5**), we combined the results across the two items in each task. Results for the DSR task revealed that the number of low-beta peaks and higher-beta peaks increased from *Delay 1.1* to *Delay 1.2*, whereas for the NEU task the number of

low-beta peaks and higher-beta peaks decreased from *Delay 1.1* to *Delay 1.2* (**Fig. 7A;** see **Supplementary Figure 9** for aperiodic component analyses). A three-way repeated measures ANOVA with factors of Task (DSR vs. NEU), Frequency Band (low-beta vs. higher-beta), and Epoch (*Delay 1.1* vs. *Delay 1.2*) revealed a significant Task x Epoch interaction, ($F(1,14) = 17.441$, $p < .001$), indicating that this divergent pattern of oscillatory peak counts between the tasks was significant. To clarify the bases of these task-level differences, we conducted follow-up paired *t*-tests comparing the peak counts for the DSR and NEU tasks within each epoch and band. These tests revealed significantly more low-beta peaks in the time-resolved RSA of the DSR task than of the NEU task during *Delay 1.2* ($t(14) = 2.779$, $p = 0.015$, $d = 0.718$), a pattern consistent with the oscillatory patterns in the behavior. Moreover, the DSR and NEU tasks showed divergent low-beta peak *shifts* from *Delay 1.1* to *Delay 1.2* ($t(14) = 2.703$, $p = .0172$, $d = .698$), driven by the significant reduction in low-beta peaks across the epochs in the NEU task ($\Delta M = -0.60$, $t(14) = -2.81$, $p = .014$). Unexpectedly, these tests also revealed significantly more higher-beta peaks in DSR representational similarity, relative to NEU, during *Delay 1.2* ($t(14) = 2.432$, $p = .029$, $d. = .628$). Although the higher-beta peak shifts from *Delay 1.1* to *Delay 1.2* diverged across tasks at a level that approached significance ($t(14) = 2.073$, $p = .0572$, $d = .535$), neither task exhibited a significant change in the number of higher-beta peaks across epochs (both *p*-values $\geqq .096$) suggesting that the temporal evolution of task-related frequency modulation in representational similarity was specific to the low-beta band.

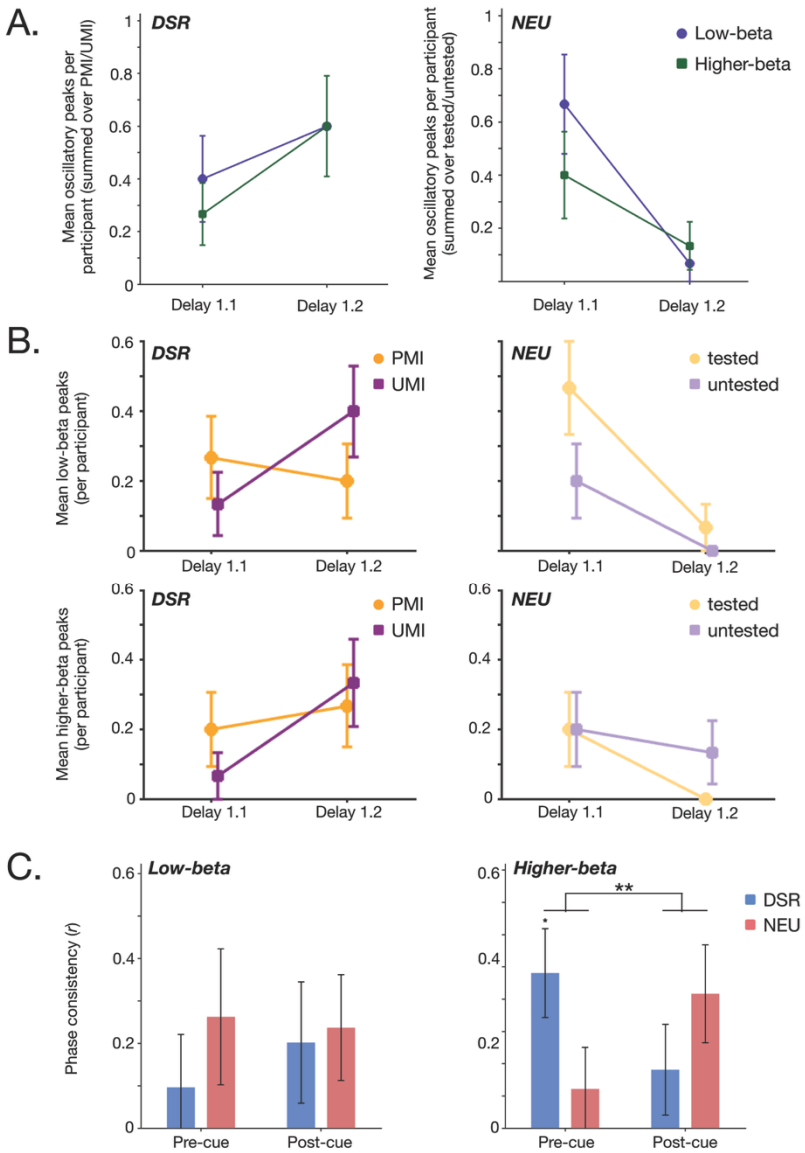

Fig 7. RSA oscillatory characteristics. A. Group-averaged mean number of low-beta peaks (indigo circles) and higher-beta peaks (green squares) per participant from *Delay 1.1* and *Delay 1.2* for the DSR task (left) and the NEU task (right). **B.** Group-averaged mean number of low-beta peaks (upper row) and higher-beta peaks (lower row) per participant from *Delay 1.1* data and *Delay 1.2* data for the DSR task (left column) and the NEU task (right column), split by memory item with PMI/tested item results in purple and UMI/untested item results in orange. **C.** Group-level phase consistency in *Delay 1.1* (pre-cue) and *Delay 1.2* (post-cue) periods for the DSR task (blue) and NEU task (red) in the low-beta band (14-16 Hz; left) and the higher-beta band (19-21 Hz; right). * permutation $p < .05$; ** permutation $p < .01$. Error bars correspond to +/- 1 *SEM* (**A.** & **B.**) and to bootstrapped 95% confidence intervals (**C.**).

Spectral analyses—beta-band peak extraction at the item level. To determine whether the frequency-specific task effects illustrated in **Figure 7A** reflected modulation of PMI representations, UMI representations, or both, we conducted separate analyses for each item type. We extracted peak counts independently for PMI, UMI, tested item, and untested item time courses and computed descriptive statistics (**Fig. 7B;** see **Supplementary Figure 10** for item-specific aperiodic component analyses). In the DSR task, PMI beta peak counts remained relatively stable across epochs for both low-beta (*Delay 1.1*: *M* = .27; *Delay 1.2: M* = .20) and higher-beta (*Delay 1.1*: *M* = .2; *Delay 1.2: M* = .27). UMI beta peak counts, in contrast, increased from *M* = 0.13 to *M* = 0.40 peaks in low-beta and from *M* = .07 to *M* = .33 peaks in higher-beta.

In the NEU task, beta peak counts declined for both the tested item and the untested item: tested (low-beta from *Delay 1.1* (*M* = .47) to *Delay 1.2* (*M* = .07), and for higher-beta from *Delay 1.1* (*M* = .2) to *Delay 1.2* (*M* = 0); untested (low-beta from *Delay 1.1* (*M* = .2) to *Delay 1.2* (*M* = 0.00) and higher-beta *Delay 1.1* (*M* = .2) to *Delay 1.2 (M* = .133).

Spectral analyses—phase relations between items. To determine whether the phase relationship between the representations of the two memory items differed as a function of task, we quantified the phase consistency (*r*) in each task and frequency band, which indicated the degree to which the cross-spectral phase angle between the two RSA time courses was consistent across participants. In the low-beta band (14–16 Hz), no significant Task × Epoch interaction was observed (permutation *p* = 0.58; **Fig. 7C**), and no individual condition showed significant phase consistency (all Rayleigh *p* > 0.35). In the higher-beta band (19–21 Hz), there was a significant Task × Epoch

interaction (permutation $p = 0.0079$). Prior to the cue, there was significant phase consistency between items in the DSR task ($r = 0.481$, Rayleigh $z = 3.47$, $p = 0.028$), but not in the NEU task ($r = 0.122$, $p = 0.81$). Following the cue, this pattern reversed: phase consistency in DSR decreased ($r = 0.181$, $p = 0.62$) and phase consistency in NEU exhibited a marginal increase ($r = 0.417$, $p = 0.072$).

Interim discussion—Experiment 2

Behavioral results broadly replicated the evidence from Experiment 1 that prioritization shields an item from the biasing influence of other information recently or currently in working memory. One possible exception to this was the fact that, unique to Experiment 2, recall of *Sample 2* showed greater repulsion from *Sample 1* in DSR than in NEU. However, we speculate that this, together with other specific differences between the two experiments, may reflect an interaction of prioritization with the longer delay period of Experiment 2. For example, previous work has suggested that longer delays (Chunharas et al., 2022), as well as “active, not passive, maintenance” (Scotti et al., 2021) are associated with greater separation between items.

Spectral parameterization of the EEG in the DSR task revealed a cue-locked increase of oscillatory peaks in the low-beta band, together with a decrease in oscillatory peaks in the higher-beta band, suggesting an oscillatory basis for the priority-specific behavioral oscillations from Experiment 1. Burst analyses indicated that these effects in these narrow frequency bands were unlikely to be due to changes of burst dynamics at the single trial level.

Results from time-resolved RSA analyses provided two important insights. First, in the DSR task, priority-related representational changes were more pronounced for the uncued item (i.e., the UMI) than for the cued item (the PMI). This suggests that at least some of the “shielding” effects of prioritization may result from representational transformations of the item that is *not* needed for the impending action. Second, although these analyses showed cue-related effects on phase dynamics, they failed to provide evidence that a strengthening of phase encoding may be a basis for priority-related shielding.

Discussion

The results from these two experiments provide evidence for a model in which the prioritization of one among two items held in working memory prompts representational transformations that are larger for the uncued item (i.e., the UMI) than for the cued item (the PMI), and in which the encoding of UMI status is implemented, at least in part, by dynamics in the beta band. Previous studies of the DSR task combining EEG and transcranial magnetic stimulation (TMS) have shown that decoding of the UMI depends on the beta band (Rose et al., 2016; Fulvio & Postle, 2025), and this effect is associated with cue- and TMS-related dynamics in the low beta band (i.e., 13-20 Hz; Fulvio et al., 2025). Furthermore, single pulses of TMS (spTMS) delivered during *Delay 1.2* can produce behavioral evidence for the involuntary retrieval of the UMI (indexed by an inflated false-alarm rate; Rose et al., 2016; Fulvio & Postle, 2020), and the magnitude of this behavioral effect is predicted by the magnitude of a spTMS-related decrease in

beta-band components derived from a decomposition of the EEG (Fulvio et al., 2024). In the present study, we have produced evidence that prioritization is associated with a behavioral oscillation in the low-beta band and by an increase of oscillatory peaks in this same narrow frequency band. Thus, our working model is that UMI status is encoded, and sustained, by a process that cycles at a frequency in the low-beta band. Although this account lacks an explicit mechanism, the RSA results from Experiment 2 do argue against the likelihood that the mechanism might be the encoding of the two memory items at different phases of a low-beta oscillation.

Although we do not yet understand the precise mechanism that implements the state of deprioritization, we speculate that its dependence on oscillations at a low-beta frequency links it to the natural frequency of thalamocortical circuits at posterior nodes of the frontoparietal priority map. This follows from the results of several studies that have recorded the EEG while spTMS is delivered to posterior parietal cortex (PPC): spTMS of PPC produces a spectral perturbation that is strongest in β1 (13-20 Hz; in comparison to spTMS of occipital cortex--alpha: 8-12 Hz--and spTMS of premotor cortex--β2: 21-29 Hz; Rosanova et al., 2009); when measured as the global mean field amplitude (GMFA), the amplitude of the response evoked by spTMS of PPC varies with pre-spTMS phase in the beta band (Kundu et al., 2014); and spTMS-evoked phosphene perception depends on pre-spTMS power in the beta band for spTMS of PPC (in comparison to its dependence on pre-spTMS power in the alpha band for spTMS of occipital cortex; Samaha et al., 2017). Assuming that priority in working memory is encoded in the frontoparietal priority map, it may be that the top-down signals that

impose this priority status on stimulus representations in early visual areas oscillate at the natural frequency of the PPC.

The behavioral and EEG data presented here point to an oscillatory mechanism supporting prioritization: recall precision oscillates at 15 Hz, and the prioritization-specific increase of oscillatory peaks in this narrow frequency band cannot be accounted for by the sparse bursting rate that we observed. This suggests that prioritization is supported by a mechanism that is fundamentally different from the beta bursts, also observed at posterior electrodes, that implement inhibitory cognitive control (e.g., Lundqvist et al., 2024; Wessel & Anderson, 2024). Importantly, however, our claim does not extend to the processes that underlie the more general function of the maintenance of information in working memory. Indeed, when we applied a burst analysis to the broader band of traditionally defined beta (15-29 Hz), we observed a burst rate comparable to one that has been shown to underlie load-related dynamics in the EEG (Kavanaugh et al., 2026).

Inspection of the time-resolved RSA suggests that both memory items undergo their priority-based representational transformation almost instantaneously upon presentation of the cue. This would be consistent with the possibility that the transformations of the PMI and UMI are triggered by a common factor, as would occur with the change of a control variable in a dynamical system. Also consistent with this possibility is the fact that trial-by-trial variation in the efficacy of the geometric transformation of the PMI and of the UMI are highly correlated, as measured with fMRI and with EEG (Wan et al., 2024). The time-resolved RSA indicates that the priority-related transformation of the UMI is larger than that of the PMI, a finding consistent with

previous fMRI studies (e.g., Yu, Teng, & Postle, 2020; Teng & Postle, 2024). We speculate that this may reflect a rotation of the UMI into an action-null subspace, whereas the PMI occupies an action-potent subspace that is only minimally different from the representational state of both memory items during portions of the trial when both are equally likely to be needed for the recall response.

References

Abdalaziz M, Redding ZV, Fiebelkorn IC. Rhythmic temporal coordination of neural activity prevents representational conflict during working memory. Curr Biol. 2023;33:1855–63. https://doi.org/10.1016/j.cub.2023.03.088

Bae GY, Luck SJ. Interactions between visual working memory representations. Atten Percept Psychophys. 2017;79(8):2376–95. https://doi.org/10.3758/s13414-017-1404-8

Bastos AM, Loonis R, Kornblith S, Lundqvist M, Miller EK. Laminar recordings in frontal cortex suggest distinct layers for maintenance and control of working memory. Proc Natl Acad Sci USA. 2018;76:201710323. https://doi.org/10.1073/pnas.1710323115

Bliss DP, Sun JJ, D'Esposito M. Serial dependence is absent at the time of perception but increases in visual working memory. Sci Rep. 2017;7(1):14739. https://doi.org/10.1038/s41598-017-15199-7

Buschman TJ, Miller EK. Serial, covert shifts of attention during visual search are reflected by the frontal eye fields and correlated with population oscillations. Neuron. 2009;63:386–96. https://doi.org/10.1016/j.neuron.2009.06.020

Chota, S., Leto, C., van Zantwijk, L., & Van der Stigchel, S. (2022). Attention rhythmically samples multi-feature objects in working memory. *Scientific reports*, *12*(1), 14703. https://doi.org/10.1038/s41598-022-18819-z

Chunharas C, Rademaker RL, Brady TF, Serences JT. An adaptive perspective on visual working memory distortions. J Exp Psychol Gen. 2022;151(10):2300–23. https://doi.org/10.1037/xge0001191

Delorme A, Makeig S. EEGLAB: an open source toolbox for analysis of single-trial EEG dynamics including independent component analysis. J Neurosci Methods. 2004;134(1):9–21. https://doi.org/10.1016/j.jneumeth.2003.10.009

Diesburg DA, Greenlee JD, Wessel JR. Cortico-subcortical β burst dynamics underlying movement cancellation in humans. eLife. 2021;10. https://doi.org/10.7554/eLife.70270

Donoghue T, Haller M, Peterson EJ, Varma P, Sebastian P, Gao R, et al. Parameterizing neural power spectra into periodic and aperiodic components. Nat Neurosci. 2020;23(12):1655–65. https://doi.org/10.1038/s41593-020-00744-x

Fiebelkorn IC, Kastner S. A rhythmic theory of attention. Trends Cogn Sci. 2019;23:87–101. https://doi.org/10.1016/j.tics.2018.11.009

Fritsche M, Mostert P, de Lange FP. Opposite effects of recent history on perception and decision. Curr Biol. 2017;27(4):590–5. https://doi.org/10.1016/j.cub.2017.01.006

Fulvio JM, Postle BR. Cognitive control, not time, determines the status of items in working memory. J Cogn. 2020;3(1):8. https://doi.org/10.5334/joc.98

Fulvio JM, Rokers B, Samaha J. Task feedback suggests a post-perceptual component to serial dependence. J Vis. 2023;23(10):6. https://doi.org/10.1167/jov.23.10.6

Fulvio JM, Haegens S, Postle BR. Single-pulse TMS affects working-memory performance via posterior beta-band oscillations. J Cogn Neurosci. 2024. https://doi.org/10.1162/jocn_a_02194

Fulvio JM, Postle BR. Effects of TMS on the decoding and electrophysiology of priority in working memory. bioRxiv. 2025. https://doi.org/10.1101/2025.09.15.676374

Gao R, Peterson EJ, Voytek B. Inferring synaptic excitation/inhibition balance from field potentials. NeuroImage. 2017;158:70–8. https://doi.org/10.1016/j.neuroimage.2017.06.078

Hakim N, Vogel EK. Phase-coding memories in mind. PLoS Biol. 2018;16:e3000012. https://doi.org/10.1371/journal.pbio.3000012

Hautekiet C, Niklaus M, Oberauer K. Susceptibility to visual interference in working memory: Different results depending on the prioritization mode? J Exp Psychol Hum Percept Perform. 2025;51(6):791–807. https://doi.org/10.1037/xhp0001315

Hervault M, Wessel JR. Common and unique neurophysiological processes that support the stopping and revising of actions. J Neurosci. 2025;45(13). https://doi.org/10.1523/JNEUROSCI.1537-24.2025

Kavanaugh BC, Vigne MM, Thorpe R, Legere C, Acuff WL, Vaughan N, et al. The association between oscillatory burst features and human working memory accuracy. J Cogn Neurosci. 2026;38(2):281–98. https://doi.org/10.1162/JOCN.a.87

Kundu B, Johnson JS, Postle BR. Prestimulation phase predicts the TMS-evoked response. J Neurophysiol. 2014;112(8):1885–93. https://doi.org/10.1152/jn.00390.2013

Lewis-Peacock JA, Drysdale AT, Oberauer K, Postle BR. Neural evidence for a distinction between short-term memory and the focus of attention. J Cogn Neurosci. 2012;24:61–79. https://doi.org/10.1162/jocn_a_00140

Lipp A, Vermeesch P. The Wasserstein distance as a dissimilarity metric for comparing detrital age spectra and other geological distributions. Geochronology. 2023;5(1):263–70. https://doi.org/10.5194/gchron-5-263-2023

Lisman JE, Idart MA. Storage of 7 ± 2 short-term memories in oscillatory subcycles. Science. 1995;313:1512–5. https://doi.org/10.1126/science.7878473

Lundqvist M, Miller EK, Nordmark J, Liljefors J, Herman P. Beta: bursts of cognition. Trends Cogn Sci. 2024. https://doi.org/10.1016/j.tics.2024.03.010

Lundqvist M, Rose J, Herman P, Brincat SL, Buschman TJ, Miller EK. Gamma and beta bursts underlie working memory. Neuron. 2016;90:1–13. https://doi.org/10.1016/j.neuron.2016.02.028

Oostenveld R, Fries P, Maris E, Schoffelen JM. FieldTrip: Open source software for advanced analysis of MEG, EEG, and invasive electrophysiological data. Comput Intell Neurosci. 2011;2011:156869. https://doi.org/10.1155/2011/156869

Panichello MF, Buschman TJ. Shared mechanisms underlie the control of working memory and attention. Nature. 2021;592:601–5. https://doi.org/10.1038/s41586-021-03390-w

Pion-Tonachini L, Kreutz-Delgado K, Makeig S. ICLabel: An automated electroencephalographic independent component classifier, dataset, and website. NeuroImage. 2019;198:181–97. https://doi.org/10.1016/j.neuroimage.2019.05.026

Piwek EP, Stokes MG, Summerfield C. A recurrent neural network model of prefrontal brain activity during a working memory task. PLoS Comput Biol. 2023;19(10):e1011555. https://doi.org/10.1371/journal.pcbi.1011555

Pomper, U., & Ansorge, U. (2021). Theta-rhythmic oscillation of working memory performance. *Psychological science*, *32*(11), 1801-1810. https://doi.org/10.1177/09567976211013045

Rosanova M, Casali A, Bellina V, Resta F, Mariotti M, Massimini M. Natural frequencies of human corticothalamic circuits. J Neurosci. 2009;29(24):7679–85. https://doi.org/10.1523/JNEUROSCI.0445-09.2009

Rose N, LaRocque JJ, Riggall AC, Gosseries O, Starrett MJ, Meyering E, et al. Reactivation of latent working memories with transcranial magnetic stimulation. Science. 2016;354:1136–9. https://doi.org/10.1126/science.aah7011

Rubner Y, Tomasi C, Guibas LJ. The earth mover's distance as a metric for image retrieval. Int J Comput Vis. 2000;40(2):99–121. https://doi.org/10.1023/A:1026543900054

Samaha J, Sprague TC, Postle BR. Decoding and reconstructing the focus of spatial attention from the topography of alpha-band oscillations. J Cogn Neurosci. 2016;28:1090–7. https://doi.org/10.1162/jocn_a_00955

Samaha J, Gosseries O, Postle BR. Distinct oscillatory frequencies underlie excitability of human occipital and parietal cortex. J Neurosci. 2017;37(11):2824–33. https://doi.org/10.1523/JNEUROSCI.3413-16.2017

Samaha J, Switzky M, Postle BR. Confidence boosts serial dependence in orientation estimation. J Vis. 2019;19(4):25. https://doi.org/10.1167/19.4.25

Scotti PS, Hong Y, Leber AB, Golomb JD. Visual working memory items drift apart due to active, not passive, maintenance. J Exp Psychol Gen. 2021;150(12):2506–24. https://doi.org/10.1037/xge0000890

Shin H, Law R, Tsutsui S, Moore CI, Jones SR. The rate of transient beta frequency events predicts behavior across tasks and species. eLife. 2017;6:e29086. https://doi.org/10.7554/eLife.29086

Siegel M, Warden MR, Miller EK. Phase-dependent neuronal coding of objects in short-term memory. Proc Natl Acad Sci USA. 2009;106:21341–6. https://doi.org/10.1073/pnas.0908193106

Sprague TC, Ester EF, Serences JT. Restoring latent visual working memory representations in human cortex. Neuron. 2016;91:694–707. https://doi.org/10.1016/j.neuron.2016.07.006

Teng C, Postle BR. Investigating the roles of the visual and parietal cortex in representing content versus context in visual working memory. eNeuro. 2024;11(2). https://doi.org/10.1523/ENEURO.0270-20.2024

van Snellenberg JX. BCa_bootstrap. MathWorks File Exchange; 2018. https://www.mathworks.com/matlabcentral/fileexchange/69119

Vergauwe, E., Hardman, K. O., Rouder, J. N., Roemer, E., McAllaster, S., & Cowan, N. (2016). Searching for serial refreshing in working memory: Using response times to track the content of the focus of attention over time. *Psychonomic bulletin & review*, *23*(6), 1818-1824. https://doi.org/10.3758/s13423-016-1038-1

Wan Q, Menendez JA, Postle BR. Priority-based transformations of stimulus representation in visual working memory. PLoS Comput Biol. 2022;18(6):e1009062. https://doi.org/10.1371/journal.pcbi.1009062

Wan Q, Ardalan A, Fulvio JM, Postle BR. Representing context and priority in working memory. J Cogn Neurosci. 2024;36(7):1374–94. https://doi.org/10.1162/jocn_a_02166

Waschke L, Donoghue T, Fiedler L, Smith S, Garrett DD, Voytek B, et al. Modality-specific tracking of attention and sensory statistics in the human electrophysiological spectral exponent. eLife. 2021;10:e70068. https://doi.org/10.7554/eLife.70068

Wessel JA, Anderson MA. Neural mechanisms of domain-general cognitive control. Trends Cogn Sci. 2024;28(2):124–43. https://doi.org/10.1016/j.tics.2023.09.008

Yu Q, Teng C, Postle BR. Different states of priority recruit different neural representations in visual working memory. PLoS Biol. 2020;18:e3000769. https://doi.org/10.1371/journal.pbio.3000769